Article

Not peer-reviewed version

Effects of Dust Storm and Wildfire Events on Phytoplankton Growth and Carbon Sequestration in the Tasman Sea, Southeast Australia

Hiep Nguyen Duc *, John Leys, Matthew L Riley, Stephen White, Merched Azzi, Toan Trieu, David Salter, Fei Ji, Huynh Nguyen, Lisa T.-C. Chang, Khalia Monk, Justine Firth, David Fuchs, Xavier Barthelemy

Posted Date: 8 January 2024

doi: 10.20944/preprints202401.0570.v1

Keywords: February 2019 Dust storm; 2019-2020 summer wildfires; Southeast Australia; phytoplankton growth; WRF-Chem model; Southern Ocean; Tasman Sea

Article

Effects of Dust Storm and Wildfire Events on Phytoplankton Growth and Carbon Sequestration in the Tasman Sea, Southeast Australia

Hiep Duc Nguyen [1,2,3,*], John Leys [3,4,5], Matthew Riley [3], Stephen White [3], Merched Azzi [3], Toan Trieu [3], David Salter [3], Fei Ji [3], Huynh Nguyen [6], Lisa Tzu-Chi Chang [3], Khalia Monk [3], Justine Firth [3], David Fuchs [3] and Xavier Barthelemy [3]

1 Laboratory of Environmental Sciences and Climate Change, Institute for Computational Science and Artificial In-telligence, Van Lang University, Ho Chi Minh City, Vietnam
2 Faculty of Environment, School of Technology, Van Lang University, Ho Chi Minh City, Vietnam
3 Department of Planning and Environment, NSW, PO Box 29, Lidcombe 2141, NSW, Australia
4 The Fenner School of Environment & Society, Australian National University, Acton, ACT 2601, Australia; johnleys58@outlook.com
5 Land and Water—Black Mountain, CSIRO, Acton, ACT 2601, Australia
6 Faculty of Engineering and Information Technology (IT), University of Technology Sydney, Ultimo, NSW 2007, Australia
* Correspondence: hiep.nguyenduc@vlu.edu.vn

Abstract: Dust storms and wildfires occur frequently in southeastern Australia. Their effects on ecology, environment and population exposure have been the focus of many studies recently. Dust storms do not emit ground-sequestered carbon but wildfires emit significant quantities of carbon into the atmosphere. However, both natural events promote phytoplankton growth in water bodies because carbon, and other trace elements such as iron, deposit on the surface water of oceans. Carbon dioxide is reabsorbed by phytoplankton via photosynthesis. The carbon balance cycle due to dust storms and wildfires are not well known. Recent studies on the carbon emission of the 2019-2020 summer wildfires in eastern Australia indicated that this megafire event emitted approximately 715 million tonnes of CO_2 (195 Tg C) into the atmosphere from burned forest areas. The projected increase in the frequency of wildfires due to climate change alters what was a carbon neutral process of reabsorbing emitted carbon by the forests, and subsequently cannot be achieved. With the result of net loss of sequestered carbon to the atmosphere, subsequently further promotes a warming climate. This study focusses on the association of dust storms and wildfires in southeastern Australia with phytoplankton growth in the Tasman Sea due to the February 2019 dust storm event and the 2019-2020 Black Summer wildfires. Central Australia and western New South Wales were the sources of the dust storm emission (11 to 16 February 2019) and the Black Summer wildfires occured along the coast of New South Wales and Victoria (from early November 2019 to early Januaray 2020). The results show the similarities and differences in the deposition of particulate matter, phytoplankton growth and carbon reabsorption patterns in the Tasman Sea from these events. Using WRF-Chem model, during the 5 days dust storm event in February 2019, approximately ~1230 tons of total dust were predicted to be deposited in the Tasman Sea while ~132,000 tons of PM_{10} were deposited in the early stage of the wildfires from 1 to 8 November 2019.

Keywords: February 2019 dust storm; 2019-2020 summer wildfires; Southeast Australia; phytoplankton growth; WRF-Chem model; southern ocean; tasman sea

1. Introduction

Emissions of dust from dust storm and smoke aerosols from biomass burnings contain organic compounds and elemental metals including iron (Fe). The deposition of dust and aerosols particles of various sizes such as $PM_{2.5}$ (particulate matter ≤ 2.5 μm in diameter) and PM_{10} (particulate matter ≤ 10 μm in diameter) on ocean increases the concentration of soluble Fe in marine water as these particles are transported from land sources over the ocean. One-third of the world oceans, and in

 doi:10.20944/preprints202401.0570.v1

particular, the high-nutrient low-chlorophyll (HNLC) Southern Ocean is mostly iron-limited in stimulating phytoplankton growth [1]. The increase in concentration of Fe stimulates the growth of phytoplankton (especially diatoms) which absorb CO_2 during photosynthesis [2]. This results in an increase of CO_2 transferred from the atmosphere into the ocean. Phytoplankton as microalgae plants contain the chlorophyll pigment. Like other land-based plants, phytoplankton grows by absorbing carbon dioxide in sea water producing glucose and oxygen through photosynthesis. Therefore, chlorophyll concentration can be used as an index of phytoplankton biomass. It is estimated that marine phytoplankton capture almost an equal amount of carbon as does photosynthesis by land vegetation [3].

The global climate change models take into account the ocean important role of carbon sequestration in the Global Carbon Cycle. Absorption of CO2 via phytoplankton life cycle is part of this process. Of the two main types of phytoplankton, dinoflagellates and diatoms, diatoms can grow quickly in Fe rich environment [4]. Recently Gregg and Rousseaux, 2019 [5] have shown that sattellite records indicated, from 1998 to 2015, the global net ocean primary production (PP), representing the uptake of inorganic carbon through photosynthesis, has experienced a small but significant decline. This is mainly due to the change in the composition of types of phytoplankton. Using sediment core record in the Southern Hemisphre, Calvo et al. 2004 [6] showed that increasing supply of dust in the Tasman Sea during the last four glacial times, with different proportion of iron and silica, induced changes in the relative contribution of the types of phytoplankton to their total productivity. Besides its role in carbon sequestration, phytoplankton growth produces dimethylsulfide which is emitted and when entered into the atmosphere can promote cloud formation and hence cool the atmosphere.

In early 2004, the European Iron Fertilization Experiment (EIFEX) stimulated a large scale diatom bloom in the Southern Ocean near Antarctica, with peaks shown in the fourth week after fertilization. This was followed by mass mortality of several diatom species and resulted in rapidly sinking aggregates of entangled cells and chains. At least half the bloom biomass sank far below a depth of 1,000 metres with a substantial portion likely to have reached the sea floor [7]. This pioneering experiment showed the important role of the ocean and particularly of phytoplankton in the CO_2 absorption as part of the carbon cycle and the ideas of geo-engineering using Fe fertilisation for CO_2 sequestration [4] [8]. The sequestration of CO_2 from surface to deep water in the Southern Ocean via the biological pump gradually increases the dissolved inorganic carbon (DIC) concentration such as $[CO_3]^{2-}$ in the oceanic carbon reservoirs.

In a study of sediment core from the Subantarctic Atlantic, Martínez-García et al. (2014) [9] found that peak glacial times and millennial cold events are characterized by increases in dust flux, consistent with Subantarctic iron fertilization. This resulted in the lowering of CO_2 at the transition from mid-climate states to full ice age conditions. Over time circulation and ventilation via the upwelling of deep-water masses can alter between a carbon sink or source. The upwelling of Circumpolar Deep Waters (CDW) in the Antarctic and Subantarctic Zones of the Southern Ocean can bring the carbon-rich waters in these reservoirs to the surface and release CO_2 to the atmosphere [10].

Recent modelling study by [11] on ocean dynamics showed that, depending on the depth at which carbon was stored, the median sequestration time driven by biological pump enhancement range from a few decades to ~150 years with a global mean value of 109 years. The Atlantic and Southern Ocean has a sequestration time shorter than the Pacific and Indian Oceans as deep upwelling occurs more frequently in the Southern Ocean. At a depth of 2100 m, more than 95% of the material remains sequestered after 50 years and at 3000 m depth, essentially 100% of the CO_2 is retained after 50 years.

The near-surface concentration of chlorophyll-a (milligrams of chlorophyll pigment/m^3) in the ocean is detected via colour change from blue to green and measured daily by sensors on polar-orbited MODIS Terra/Aqua satellites with high resolution at 1km x 1km and geostationary Himawarri satellite over Australia to Japan at time resolution of minutes. Phytoplankton grows when nutrients, including Fe, in the water are sufficient and temperature and light are favourable. If too much nutrients are present, this will result in high growth and higher concentration of phytoplankton. Some species of phytoplankton can produce toxin build up, causing the algal bloom

 doi:10.20944/preprints202401.0570.v1

to deplete oxygen concentrations and can be deadly to marine life and even people on land-based water bodies

The composition of pollutants in the dust can also influence the solubility of Fe. Rodriguez et al. 2021 [12] studied the changing concentration of soluble Fe across the Atlantic Ocean from a dust storm outbreak in North African and found that dust mixing with acid pollutants increases the solubility of Fe. Dust storms from different sources therefore have different effects on the receiving water bodies which themselves have different characteristics including nutrient levels. Lauderdale et al. 2020 [13] have recently shown that Fe fertilisation in the Southern Ocean, where rich nutrients such as nitrate and phosphate are readily available, overall cannot reduce atmospheric CO_2 and therefore mitigate climate change as the world oceans are interconnected. For example, an increase of phytoplankton growth in the Southern Ocean due to iron fertilisation, can reduce the availability of macronutrients in the North Atlantic and therefore reduce the phytoplankton growth there. Perron et al. 2020 [14] have shown that dust-sourced high Fe loadings and low Fe solubilities (5%) aerosols dominate the atmospheric burden of the western coasts of Australia. However, much lower Fe concentrations but greater Fe solubilities (10.5% and 13%) in aerosols along the east coast which was attributed to solubility-enhancing atmospheric reactions with anthropogenic pollutants. In northern Australia, high aerosol Fe solubilities (>20%) were associated with direct emissions or atmospheric reactions with bushfire emissions at tropical latitudes.

For some of the most significant dust storms on the east coast Australia such as the September 2009 '*Red Dawn*' dust storm event, Gabric et al. 2015 [15] found that surface chlorophyll concentrations in the southern Tasman Sea during the austral spring of 2009 were well above the climatological mean, with positive anomalies as high as 0.5 mg m^{-3}. Earlier dust storms in late 2002 and early 2003 were also studied by Gabric et. al. 2010 [16] using satellite data and the integrated wind erosion and dust transport model (CEMSYS) to simulate the daily deposition during November 2002 to February 2003. They found that during February 2003 there was strong evidence for a large-scale natural dust fertilization event in the Australian sector of the Southern Ocean.

The most recent major dust storm occurred in February 2019. In the austral summer of 2019, from 11 and 15 February 2019, under persistent westerly and south westerly winds, a dust storm started in the deserts of Central Australia carried large volume of dust in an extensive front of approximately 1500 km moving to the western region of the state of New South Wales (NSW) then to the coast including the metropolitan area of Sydney causing extreme high particle pollution. The dust continued to be transported across the Tasman Sea to New Zealand and to Antarctica [17]. This study will examine the effect of the February 2019 dust storm on the phytoplankton growth in the Tasman Sea.

Dust deposition by far is the largest source of Fe in the ocean basins, more than the pyrogenic sources (fires and anthropogenic combustion). In a study on the trend of soluble Fe deposition from these sources based on satellite data from 1980 to 2005, Hamilton et al. 2020 [18] showed that dust iron decreases while fire iron slightly increases and anthropogenic iron has a significant increasing trend.

While dust iron dominates the absolute deposition magnitude, wildfire iron is an important contributor to temporal variability. The recent large wildfires on the East Coast of Australia in late spring and summer period of 2019/2020 (Black Summer wildfires) has been shown by Tang et al. 2021[19] to contribute significant growth of phytoplankton in the Pacific and South Australia parts of the Southern Ocean.

The Black Summer 2019/2020 wildfires event in southeast Australia was unprecedented in terms of scale or intensity, duration of the fires and their spatial extent. With a prolonged drought in 2019, low soil moisture and increasing fuel load, the wildfires started in the northern coastal areas of NSW and the Blue Mountains areas of the state of NSW from late October, November to December 2019. Then the wildfires occurred in the south coast of NSW, moving south to the coastal border areas between NSW and the state of Victoria and finally in the East Gippsland of Victoria in early January 2020 [20] . The 2019/2020 wildfires totally burned 5.68 million ha in NSW and 1.58 million hectares (ha) in Victoria [21] (Davey et al. 2020), and thirty-three people lost their lives [22] (AIHW, 2020). The

 doi:10.20944/preprints202401.0570.v1

megafire of 2019/2020 emitted approximately 400 megatons (trillion or 10^{12} grams) of CO_2 into the atmosphere as estimated by ECMWF (European Centre for Medium-Range Weather Forecasts) [https://atmosphere.copernicus.eu/wildfires-continue-rage-australia][23]. Smoke aerosols rose to the upper troposphere more than 5km above ground and even to the stratosphere travelling at high speed to the South Pacific, South America to South Africa and back to the Australian continent. The effect of the megafires was compared to those of volcanic eruptions which influenced the ENSO development cycles and hence had far reaching effect on the climate in many regions around the world [24] . Using coupled climate model ensembles based on the Community Climate System Model version 2 (CESM2), Fasullo et al. 2023 [24] has shown that the aerosol effect in the South Pacific from cloud formation and reflection cooled the atmosphere and the ocean surface temperature and prolonging the La Nina phase of the ENSO cycle. Our study will focus on the effect of the early stage of Black Summer wildfires in early November 2019 on the dispersion and deposition of smoke aerosols associating with the phytoplankton growth and the subsequent carbon sequestration in the Tasman Sea.

To estimate the dispersion, transport and deposition of pollutants from the air to surface level from dust or wildfires events, air quality models are often used. The two most common models are WRF-Chem and WRF-CMAQ. The WRF-CMAQ air quality model was used by many authors to study the deposition of pollutants. Qiao et al. 2015 [25] has used WRF-CMAQ to study dry and wet deposition of sulfate, nitrate, and ammonium ions in Jiuzhaigou National Nature Reserve (China). Van der Velde et al. 2021 [26] has used WRF-Chem v.4 to estimate the emission and concentration of CO and CO_2 over eastern Australia during the 2019-2020 wildfires based on 5 different fire emission inventories where emission estimate was constraint by CO satellite measurements. WRF-Chem v.4 was also used to study the effect of the 2019/2020 wildfires on air quality and health in east coast of Australia [16] and the transport of dust from the February 2019 dust storm to the Tasman Sea and Antarctica [17].

WRF-Chem with different dust emission schemes have been used to account for the dust emission and deposition in air quality dispersion model over a simulation domain [27] [28]. The emission of dust created from wind erosion of land surface is described as a function of wind speed threshold, the soil characteristics such as its type or texture and moisture content and the dust source function (DSF) which describes the spatial erodibility of land surface. This erodibility factor of the land depends on the land cover, more specifically sediment supply. There are a number of methods to determine the erodibility at each location based on various hypotheses. The most common one is the topographic hypothesis which calculates the erodibility (or sediment supply) based on elevation in which topographic depressions are the largest sources of dust. This DSF based on topographic hypothesis is called the Ginoux dust source function [29]. There are other hypotheses such as the geomorphic one which describes erodibility as a function of upstream catchment area; the hydrologic hypothesis in which erodibility is described as a function of upstream flow and finally the levelness hypothesis which assumes that low-slope areas are most conducive to dust formation [30]. The DSF used by the dust emission scheme options in the WRF-Chem air quality model is based on topographic hypothesis.

In this study, the dust storms of February 2019 and the early stage of Black Summer 2019-2020 wildfires events in early November 2019 and their effects on atmospheric and marine environment are studied by using WRF-Chem 4.2 air quality model to determine their impact on phytoplankton growth in the Tasman Sea. The model is used to simulate the dust fluxes generated from wind erosion, the dust transport and dispersion in the atmosphere as well as the dust deposition on land surface or ocean. Similarly, the wildfires event of summer 2019-2010 on east coast of Australia was simulated using WRF-Chem and FINN (Fire Emission Inventory from NCAR) emission datasets [20]. The effects of these events on the biological processes in the Tasman Sea and beyond have not been examined before. temporal and spatial quantities of $PM_{2.5}$, PM_{10} and total dust from wildfires and dust emitted from These natural events and their deposition of particulate matter on the Tasman Sea off the southeast coast of Australia will be estimated from the simulation. The simulated results from both models will be compared with the observed patterns of phytoplankton growth as measured by

Preprints (www.preprints.org) | NOT PEER-REVIEWED | Posted: 8 January 2024 doi:10.20944/preprints202401.0570.v1

polar-orbited MODIS Aqua/Terra and geostationary Himawarri satellites and the phytoplankton data product from the Climate Change Initiative (CCI) – Ocean Color of the European Space Agency (ESA) . From these comparisions, the link and relationship between particle deposition and phytoplanckton growth over time will be determined.

2. Material and Methods

In this study we use the WRF-Chem V4.2 to simulate the dust events of February 2019. The WRF-Chem dust emission scheme used is the AFWA (Air Force Weather Agency of the US) version of GOCART (Goddard Chemistry Aerosol Radiation and Transport) model that we have used in our previous study of dust transport from Australia to New Zealand and Antarctica [17]. This dust emission scheme is one of several dust emission options available in WRF-Chem. In AFWA-GOCART emission scheme (dust_opt=3), the emission fluxes for the 5 particle size bins are stored in 4-dim DUST1, DUST2, DUST3, DUST4 and DUST5 variables with unit in μg/kg-dry air. The dust emission calculated over the domain is calculated as follows [31].

The accumulated dust emission (kilograms per cell) from each surface grid cell are given by:

$$EmisDUST1_{i,j} = \sum_{t=1}^{n} DUST1_{i,j} \times S_{i,j} \times \rho$$

where Emis $DUST1_{i,j}$ is the dust flux at the surface for bin 1 at grid cell (i,j) and t is the time step from 1 to n, $S_{i,j}$ is the cell surface area (m^2) and ϱ is the air density.

Similarly, the gravitational settling (Grav. Settled DUST1, kg) and dry deposition (Dry deposited DUST1, kg) is calculated for dust bin 1 are

$$Grav.Settled\ DUST1_{i,j} = \sum_{t=1}^{n} GRASET\_1_{i,j} \times S_{i,j} \times \rho$$

$$Dry\ Deposited\ DUST1_{i,j} = \sum_{t=1}^{n} DRYDEP\_1_{i,j} \times S_{i,j} \times \rho$$

In WRF-Chem, the default registry does not have gravitational settled dust and dry deposited dust in the output stream. To include these variables in the WRF-Chem output, in the time control section of the namelist.input file, the field < iofields_filename> referencing to the file containing these variables is added. The options for the deposition are set (gas_drydep_opt and aer_drydep_opt are set to 1).

For gaseous and other particles, by multiplying the deposition velocity with the concentration at a particular time and space will give the downward fluxes of these pollutants. The deposition velocity, v_d, is proportional to the sum of aerodynamic resistance, sublayer resistance and surface resistance. The parameterisation of the surface resistance most often used is the Wesely model [32] which is implemented in WRF-Chem. The Wesely model specified the surface resistance as the sum of the resistances of the soil surfaces and the vegetation which can be determined from land use data.

The wildfires event simulation is performed using WRF-Chem with fire emission data from FINN. In the previous study [20], the simulation of the Black Summer wildfires 2019-2020 event was shown to be performing well in term of air quality prediction. This study uses the same domain configuration and chemistry option (MOZCART) as in the previous simulation study but includes extra deposition variables as described above to estimate the deposition of $PM_{2.5}$ and PM_{10} which contain trace particles such as Fe. We assume that the amount of Fe is proportional to the amount of $PM_{2.5}$ and PM_{10}. The deposition velocity is used to estimate the particle flux to the ground. The domain configuration and the physics/chemistry options in WRF-Chem model for this study are given in Figure 1 and Table 1.

Preprints (www.preprints.org) | NOT PEER-REVIEWED | Posted: 8 January 2024 doi:10.20944/preprints202401.0570.v1

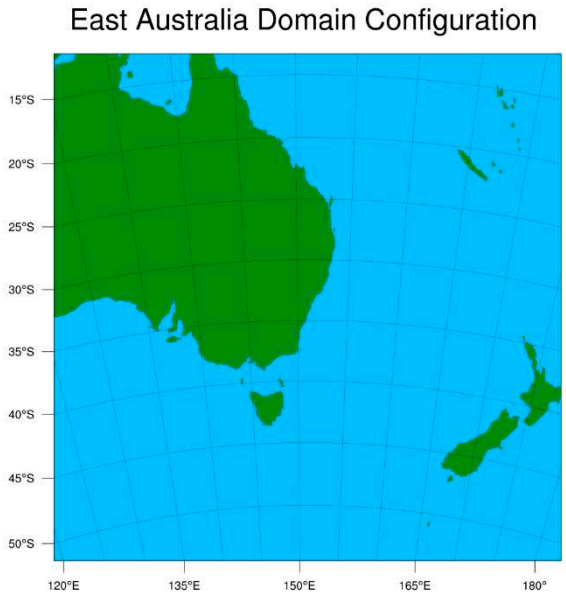

Figure 1. WRF-Chem simulation domain configuration.

Table 1. WRF-Chem physics and chemistry parametrisation.

WRF-Chem Physical parametrisation	Namelist variable	Option	Model/scheme
Microphysics	mp_physics	3	WRF Single Moment
Land surface	sf_surface_physics	2	Unified Noah Land-Surface Model
Surface layer physics	sf_sfclay_physics	1	Monin-Obukhov similarity
Planetary Boundary Layer	bl_pbl_physics	1	Yonsei University Scheme (YSU)
Shortwave radiation	ra_sw_physics	4	Rapid Radiative Transfer Model for GCM (RRTMG)
Long wave radiation	ra_lw_physics	4	Rapid Radiative Transfer Model for GCM (RRTMG)
Cloud cumulus	cu_physics	1	Kain–Fritsch Scheme
Chemistry mechanism	chem_op	112	MOZART/GOCART chemistry/aerosol scheme
Dust emission	dust_opt	3	GOCART/AFWA dust emission
Photolysis	phot_opt	3	Madronich F-TUV photolysis
Gas dry deposition	gas_drydep_opt	1	Include dry deposition of gas species
Aerosol dry deposition	aer_drydep_opt	1	Include dry deposition of aerosols
Sea salt emission	seas_opt	1	GOCART sea salt emission
Biomass burning emission	biomass_burn_opt	2	Include biomass burning emissions and plume rise calculation for MOCART
Aerosol radiation feedback	aer_ra_feedback	1	Include feedback from the aerosols to the radiation schemes
Aerosol optical property	aer_op_opt	2	aerosol optical properties calculated based upon Maxwell approximation

Spatial data on chlorophyll-a was obtained from NASA MODIS Aqua/Terra satellite chlorophyll-a product and from Himawarri geostationary satellite of Japan Aerospace Exploration Agency (JAXA). The Ocean Colour - Climate Change Initiative (OC-CCI) Project by the European Space Agency (ESA) in 2019 provided a merged multi-sensor record spanning 22 years timeseries of

Preprints (www.preprints.org) | NOT PEER-REVIEWED | Posted: 8 January 2024 doi:10.20944/preprints202401.0570.v1

chlorophyll-a data from various satellite products of reflectance sensors. The OC-CCI data can be downloaded from https://rsg.pml.ac.uk/thredds/ncss/grid/CCI_ALL-v5.0-8DAY/dataset.html

3. Results

3.1. Dust storm of 12-16 February 2019

Remote sensing data from polar-orbited MODIS Aqua/Terra satellites and geostationary Himawarri satellite before and after the dust storm event provide observation on chlorophyll-a concentration in the Tasman Sea between Australia and New Zealand which are used to correlate with the dust deposition patterns. The dust storm of 12 to 16 February 2019 originated in desert areas of Lake Eyre in Central Australia on 11 February 2019. The dust cloud reached the eastern coast of Australia in the state of NSW on the 12th February and lasted until the 14th February in the Tasman Sea. Aftterward it subsided as the dust was transpored to New Zealand. Air quality monitoring stations on NZ South Island detected high $PM_{2.5}$ concentration when the dust intruded to ground level as it travelled further south to Antarctica and the South Pacific [17] .

The progress of the dust storm from the sources in Central Australia, western New South Wales to the east coast of Australia, across the Tasman Sea to New Zealand and Antarctica was analysed in detail by [17]. Appendix A shows the simulation results of dust storm progress from Central Australia to the Tasman Sea with overlay wind field. The majority of the dust is transported to north of Australia and Western Australia while some dusts were also transported to the east coast of Australia and the Tasman Sea. In the Southern Ocean, most observed AOD was due to sea salt aerosols.

It has been shown by [17] that the dust, in this February 2019 dust storm, was being able to be transported far from the sources to the Tasman Sea, New Zealand and Antarctica because of the presence of the Great Dividing Range along the south eatern coast of Australia. The westerly wind carrying dust from sources, west of the mountain range, crossed the mountain range and hence brought the airborn dust high above the troposphere. This high altitude dust was then transported beyond the Australian mainland to New Zealand and beyond. The role of the Great Dividing Range as a launch pad for wind-born dust on its western side plays an important role in long-range transport of Ausralian dust during the dust storms.

Figure 2 shows the AOD and chlorophyll-a over Australia during the dust storm from 12 to 16 February 2019 as detected by MODIS Terra/Aqua satellites. The sensors onboard the Himawarri geostationary satellite also provided real-time chlorophyll-a concentration over the Pacific Ocean from Japan to Australia. The Himawarri processed data from JAXA (Japan Aerospace Exploration Agency) are at temporal resolution (10-minutes, 1 hour, daily and monthly) and more detailed than those from polar orbital MODIS Aqua/Terra satellites. Figure A2 in Appendix B shows the AOD and chlorophyll-a concentration as detected by Himawarri geostationary satellite on 14, 15 and 16 February 2019. Also shown in Figure A2 (g) is the anomaly of chlorophyll-a concentration in first half of February 2019 from average period 2002-2010 after the dust storm. The AOD and chlorophyll-a data products from both NASA and JAXA correspond well with each other.

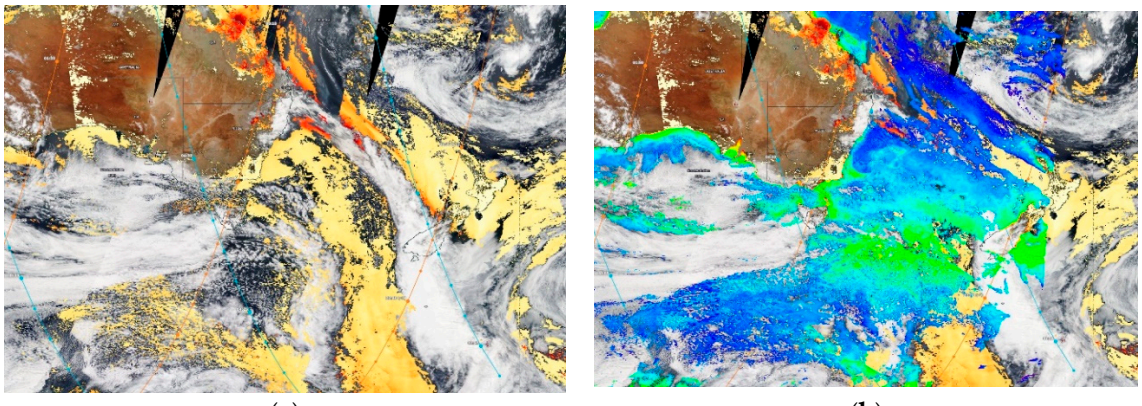

(**a**) (**b**)

Preprints (www.preprints.org) | NOT PEER-REVIEWED | Posted: 8 January 2024 doi:10.20944/preprints202401.0570.v1

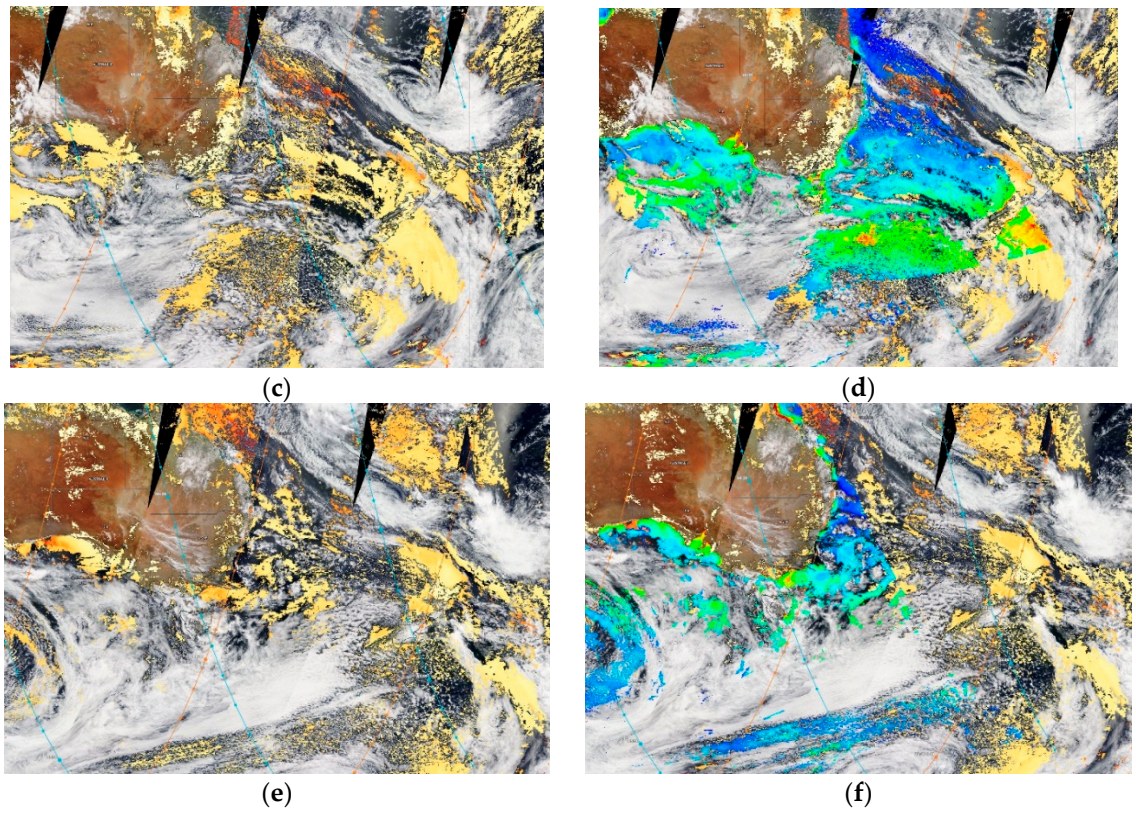

Figure 2. AOD and chlorophyll-a on 14 February 2019 (a) (b), 15 February 2019 (c) (d) and 16 February 2019 (e) (f) as detected by MODIS Terra/Aqua satellites (source: NASA Worldview AOD and chlorophyll-a MODIS products).

As the phytoplankton growth only occurred after the dust deposition on the ocean under favourable conditions, the change in chlorophyll-a concentration in February 2019 as compared to the previous years (2002-2010) at similar time is obtained as anomaly map shown in Figure A.2(g). Note that the biomass burnings and forest fires in Indonesia and South East Asia mainland and South America during this period also contributed to the growth of phytoplankton in the Indian Ocean and Pacific Ocean.

To determine the causal relationship between the dust storm and the phytoplankton growth in the Tasman Sea, the simulated dust deposition over the Tasman Sea between Australia and New Zealand for the period from 12 February 2019 to 15 February 2019 will be compared with observed chlorophyll-a data. The spatial and temporal high resolution data product of Climate Change Initiative (CCI) – Ocean Color from the European Space Agency (ESA) combines various data sources including those of NASA products such as NASA OBPG SeaWiFS, NASA OBPG VIIRS L1 R2018.0, NASA OBPG MODIS Aqua L1 R2018.0. These observed climate variables including chlorophyll-a are provided on an accessible and flexible open data portal platform for climate change research. This high quality and resolution global data set is subsetted for the Autralian domain and downloaded to be used as observed chlorophyll-a data in comparision with predicted deposition of dust on the ocean surface.

The daily chlorophyll-a data at 1km resolution from ESA Ocean Colour database for the period of 11 to 15 February 2019 are obtained and analysed for the spatial domain between lat[-24,-50] and lon[142, 179.9] encompassing the whole Tasman Sea as shown in Figure 3. This domain covers the whole Tasman Sea. The mean Chlor_a concentration varies between 0 to 0.5 $\mu g/m^3$ in the Tasman Sea between the south east coast of Australia and New Zealand. Below latitute -45^o S, the high concentration of chlorophyll-a was due to phytoplankton growth in the Southern Ocean not connected with partial dust-related phytoplankton growth in the Tasman Sea above. This can be seen in the spatial plot of the difference of daily chlorophyll-a concentration and the previous daily concentration for each day on 12, 13 and 14 February 2019. This daily difference plot represents the

Preprints (www.preprints.org) | NOT PEER-REVIEWED | Posted: 8 January 2024 doi:10.20944/preprints202401.0570.v1

new growth of phytoplankton for this day or an increase in chlorophyll-a concentrations as compared to the previous day. As the days progresed, the pattern of the new phytoplankton growth moved from the south west to the north-east direction.

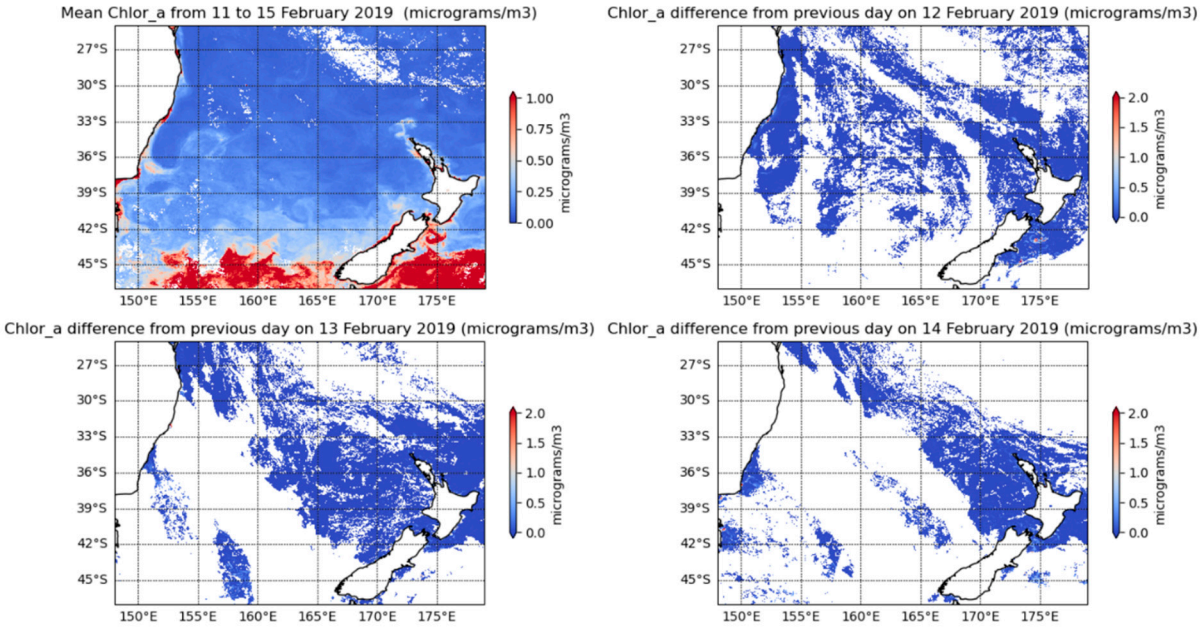

Figure 3. Mean Chlor-a concentration (µg/m3) in the Tasman Sea between Australia and New Zealand and Chlor-a concentration difference from previous day on 12, 13 and 14 February 2019. (Chl-a V5 data from European Space Agency – Ocean Colour https://www.oceancolour.org/portal/#Accessed 23 December 2023).

The WRF-Chem simulation results of the deposition rate of total dust of different sizes (0.2 - 20 µm) each day from 12 to 15 February are shown in Figure 4. The dust deposition pattern gradually moved from south west to north east which corresponds to the patterns of the chlorphyll-a growth or phytoplankton growth.

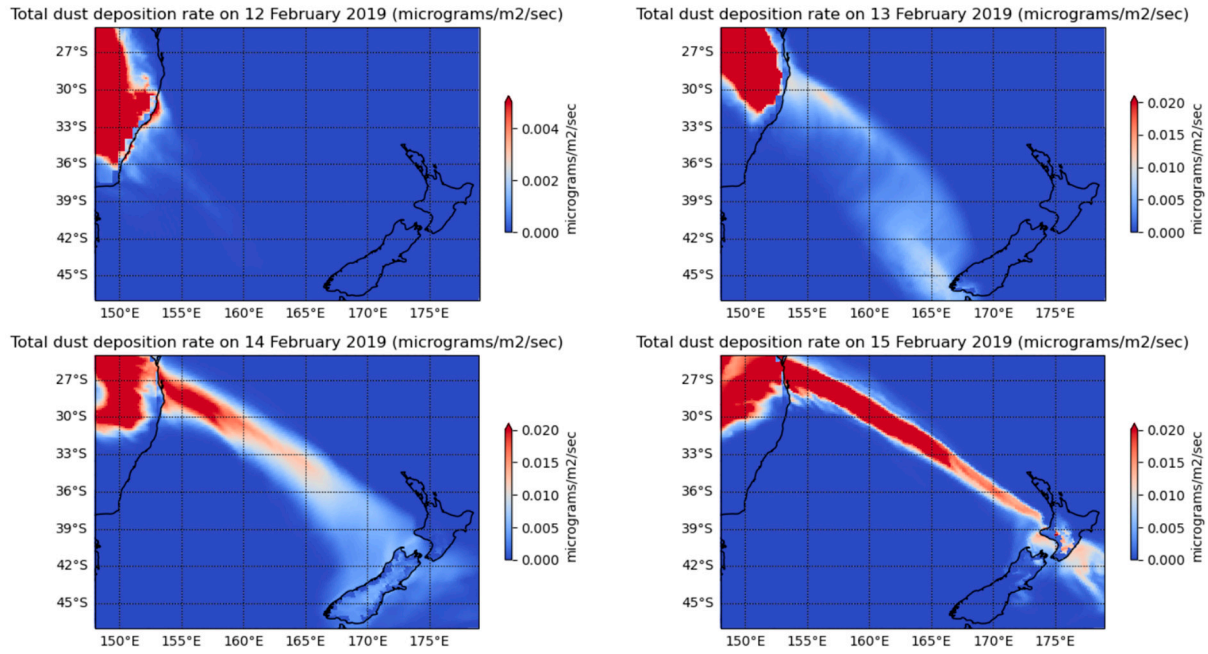

Figure 4. Total dust deposition rate in µg/m²/sec on the sea surface as predicted from WRF-Chem model on the 12, 13, 14 and 15 February 2019.

Preprints (www.preprints.org) | NOT PEER-REVIEWED | Posted: 8 January 2024 doi:10.20944/preprints202401.0570.v1

The results of the simulation of WRF-Chem 4.1 for the period 11 to 15 February 2019 provides the spatial extent and the amount of dust particles deposition over the domain. Figure 5 summarises the results of the deposition of total dust and $PM_{2.5}$ over the domain during the period of simulation. The mean deposition rate is obtained by averaging over the simulation period of the result of the multiplication of the deposition velocity and ground concentration of total dust or $PM_{2.5}$.

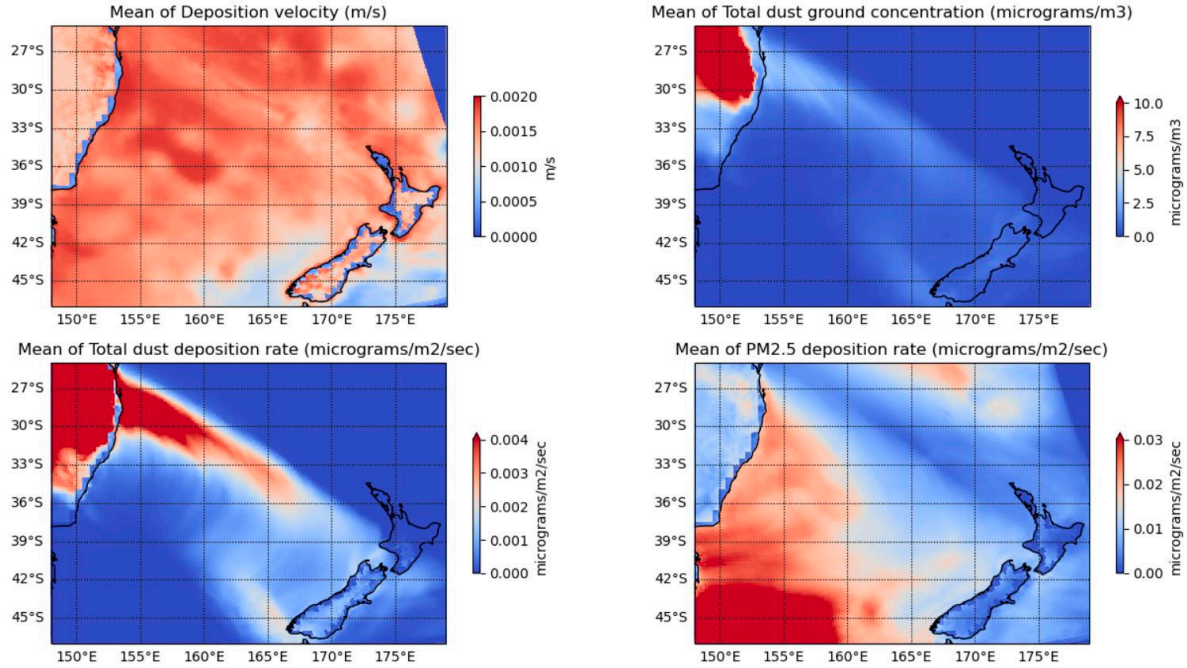

Figure 5. Mean deposition velocity (m/s) (top left), mean of total dust ground concentration ($\mu g/m^3$) (top right). Mean of total dust deposition rate ($\mu g/m^2/s$) (bottom left) and mean of $PM_{2.5}$ deposition rate ($\mu g/m^2/s$) (bottom right). $PM_{2.5}$ aerosols in the Southern Ocean are mostly composed of sea salt and of non-dust origin.

Time series of chlorophyll-a concentration at some points near the coast where high deposition of dust occurred and chlorophyll-a concentration are available. Shaw et al. 2008 [33] in their study of the effect of dust deposition from the 23 October 2002 dust storm on phytoplankton growth in Queensland coastal waters found that the high deposition of dust corresponds to the day when chlorophyll-a concentration is high. We also found that at point location near the NSW coast where high deposition rate occurred on the 12 and 13 February 2019, the chlorophyll-a concentration is also high as shown in Figure 6.

Preprints (www.preprints.org) | NOT PEER-REVIEWED | Posted: 8 January 2024 doi:10.20944/preprints202401.0570.v1

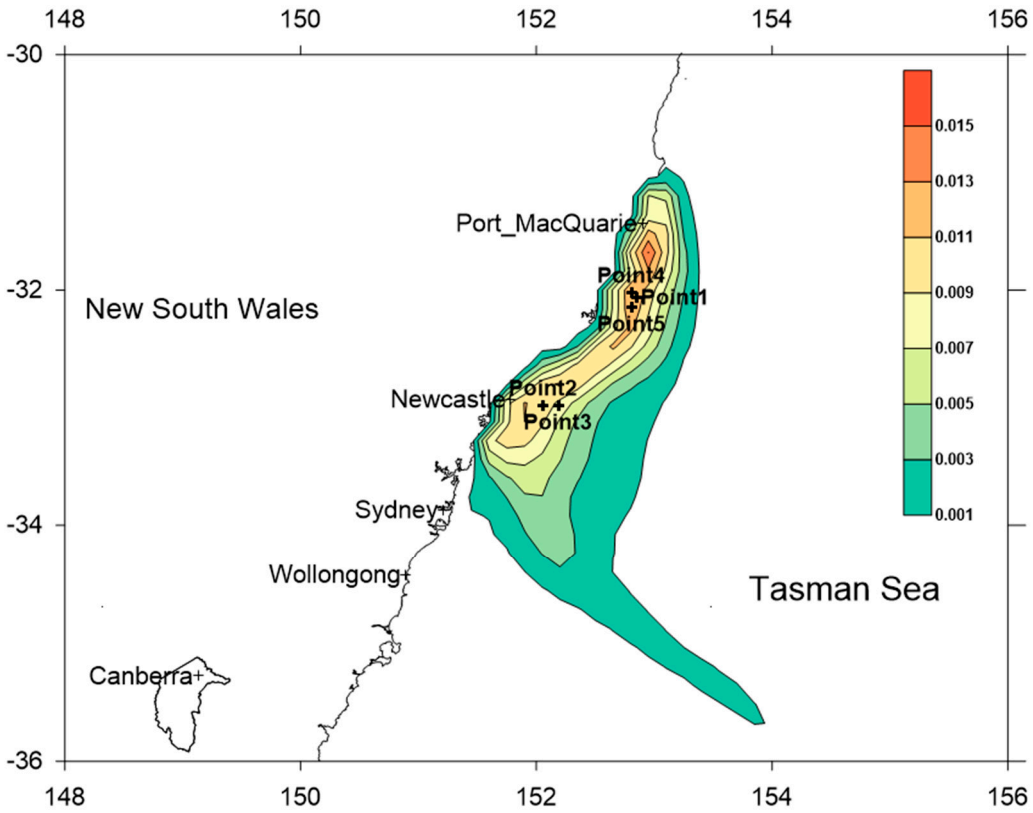

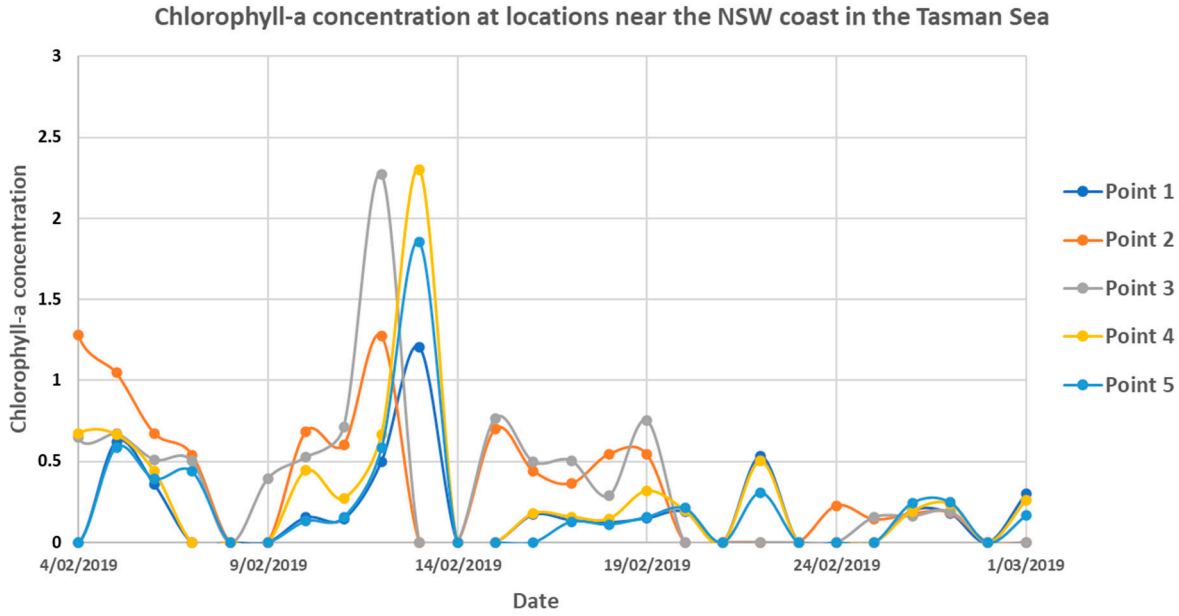

Preprints (www.preprints.org) | NOT PEER-REVIEWED | Posted: 8 January 2024 doi:10.20944/preprints202401.0570.v1

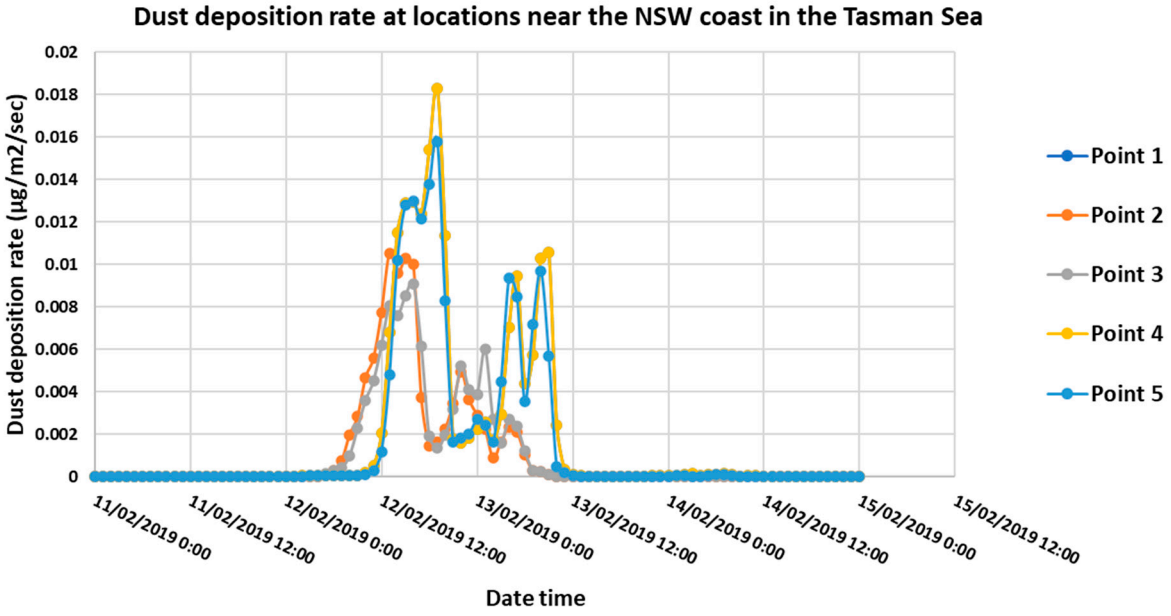

Figure 6. Dust deposition rate (µg/m^3) contour over the ocean on 12 February 2019 16 UTC and 5 point locations (a). Time series of chlorophyll-a concentration at 5 point locations along the coast of NSW from 4 to 28 February 2019 (b) where high concentration occurred on the 12 or 13 of February 2019. Time series (hourly) of predicted dust deposition rate at 5 point locations (c) where high dust deposition rates occurred on 12 and 13 February 2019. Coordinates of the point locations: Point 1 (152.854, -32.0625), Point 2 (152.062, -32.9792), Point 3 (152.188, -32.9792), Point 4 (152.812,-32.0208), and Point 5 (152.812,-32.1458).

Masking out the land mass feature, the estimated dust deposition in the Tasman Sea from WRF-Chem simulation is calculated to be approximately 1,230 tons of dust for 3 days from 12 to 15 February 2019 when the dust reached the Tasman Sea. The figure for dust deposit on land in the Australian simulation domain is about 135,000 tons which is about 10 times more than that on the Tasman Sea. The estimated accumulated total dust emission from Central Australia from 11 to 15 February 2019 is approximately 2.4 million tons of soil dust.

3.2. Wildfire's event, Black Summer 2019-2020 wildfires

The simulation of the early stage of the Black Summer 2019-2020 wildfires event from 1 to 8 November 2019 was performed using WRF-Chem air quality model to determine the emission and transport of pollutants and their effects on environment including air quality in the atmosphere and in the marine system. In terms of the effect on greenhouse emissions, wildfires have more impact than dust storms as they emit large amount of CO_2 into the atmosphere.

Van der Velde et al., 2021 [26], has estimated the amount of CO_2 emission in the Australian Black Summer wildfires to be 715 teragrams (range 517–867 trillion grams) from November 2019 to January 2020 based on 5 different fire emission inventories: Global Fire Emission Database version 4s (GFED4s), the Fire Inventory from NCAR version 1.5 (FINN); Global Fire Assimilation System version 1.2 (GFAS), Quick Fire Emissions Data set version 2.4 (QFED), and Fire Energetics and Emission Research version 1.0 (FEER). The estimations are then constrained by CO measurement from TROPOspheric Monitoring Instrument (TROPOMI5) satellite. The CO_2 emission of the 2019-2020 wildfires surpasses Australia's normal annual fire and fossil-fuel emissions by 80%. In their study of the effect of the 2019-2020 wildfires on phytoplankton growth, Tang et al. 2021 [19] have identified strong association of the AOD from this wildfires event above the Southern Ocean, south of Australia, and above the Pacific Southern Ocean (between New Zealand and South America) with the chlorophyll-a concentration in those ocean areas.

Preprints (www.preprints.org) | NOT PEER-REVIEWED | Posted: 8 January 2024 doi:10.20944/preprints202401.0570.v1

Figure A3 in the Appendix C shows the monthly average chlorophyll-a concentration as detected by Himawarri sensor in December 2019 and January 2020 as compared with those of the previous year. Note that Himawarri geostationary satellite does not cover the region beyond east of New Zealand near the International Date Line. A relative increase in chlorophyll-a concentration can be seen in the Tasman Sea and Southern Ocean south of Australia. However, a clearer indication of phytoplankton blooms is shown by plotting the anomaly chlorophyll-a concentration across the southern hemisphere, including the Pacific part of the Southern Ocean, as shown in Figure 7. The images show massive phytoplankton growth from high chlorophyll-a concentration over most of water bodies in the southern hemisphere from Australia to South America, South Africa and back to Australia. This massive growth of phytoplankton lasted from January to early March 2010.

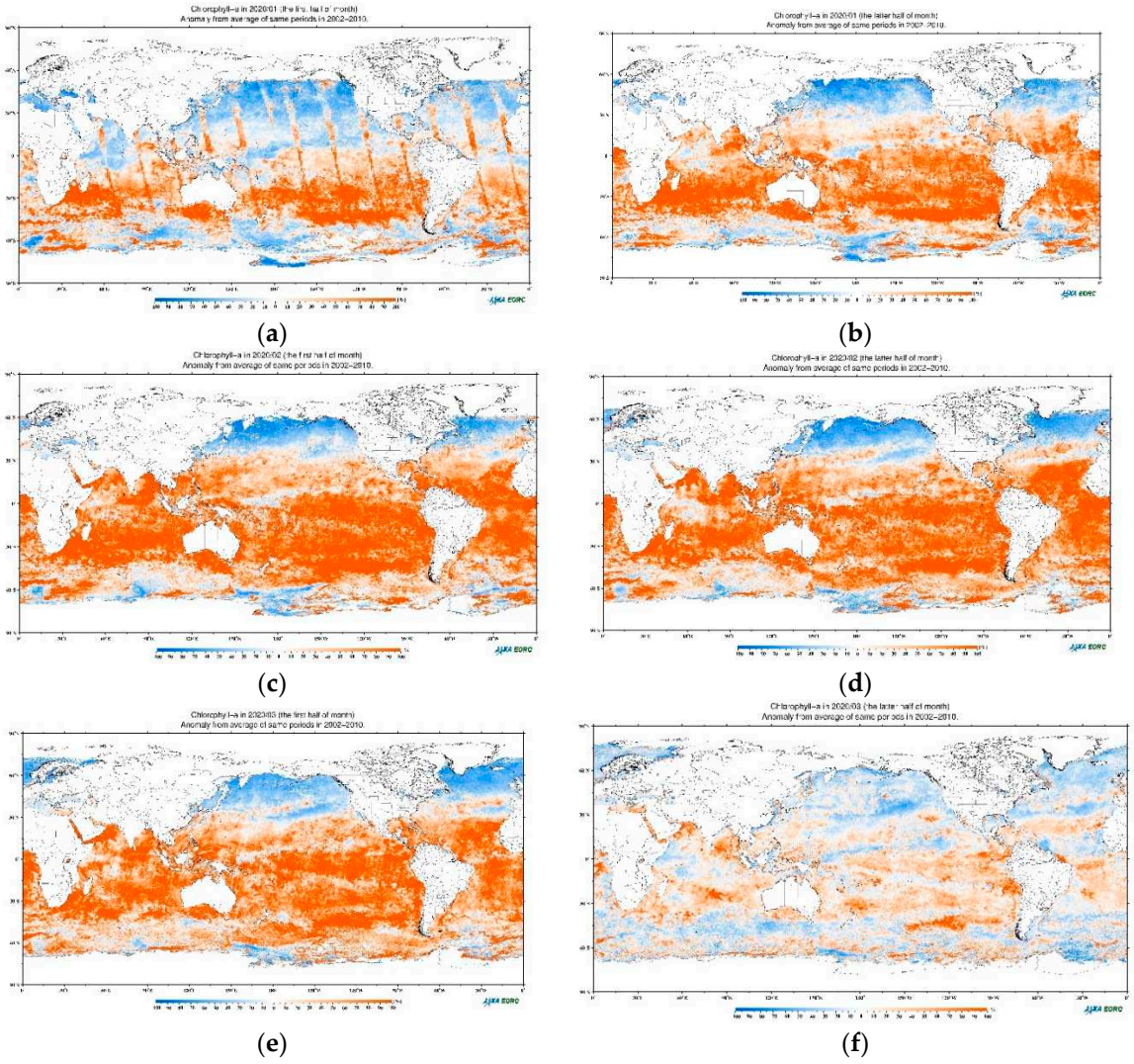

Figure 7. Chlorophyll-a anomaly in January, February and March 2020 from the same period in 2002-2010. First half of January 2020 (a), later half of January 2020 (b). First half of February 2020 (c), second half of February 2020 (d). First half of March 2020 (e) and second half of March 2020 (f) (source: JAXA Satellite Monitoring for Environment Studies, https://www.eorc.jaxa.jp/cgi-bin/jasmes/monthly/jasmes_list_v3.cgi?area=GL&lang=en&prod=CHLA&type=anomaly&year=2020).

WRF-Chem simulation in early November 2019, when the wildfires started, showed the transport of smoke aerosols and deposition of $PM_{2.5}$ and PM_{10} are shown in Figures 8 and 9. The depostion on the Tasman Sea occured due to smoke aerosols from the wildfires in northern NSW at this time. The major files in the Blue Mountains in NSW, the border areas between NSW and Victoria, and the Gipsland areas of Victoria were not yet started until late November and December 2019.

Preprints (www.preprints.org) | NOT PEER-REVIEWED | Posted: 8 January 2024 doi:10.20944/preprints202401.0570.v1

The location of the fires in early November is in northern NSW and shown in Figure 8 where the fire emission of pollutants were obtained from FINN (Fire Emission Inventory from NCAR). This emission data is crucial in the simulation using air quality model to predict the dispersion and concentration of pullutants at different high in the atmosphere.

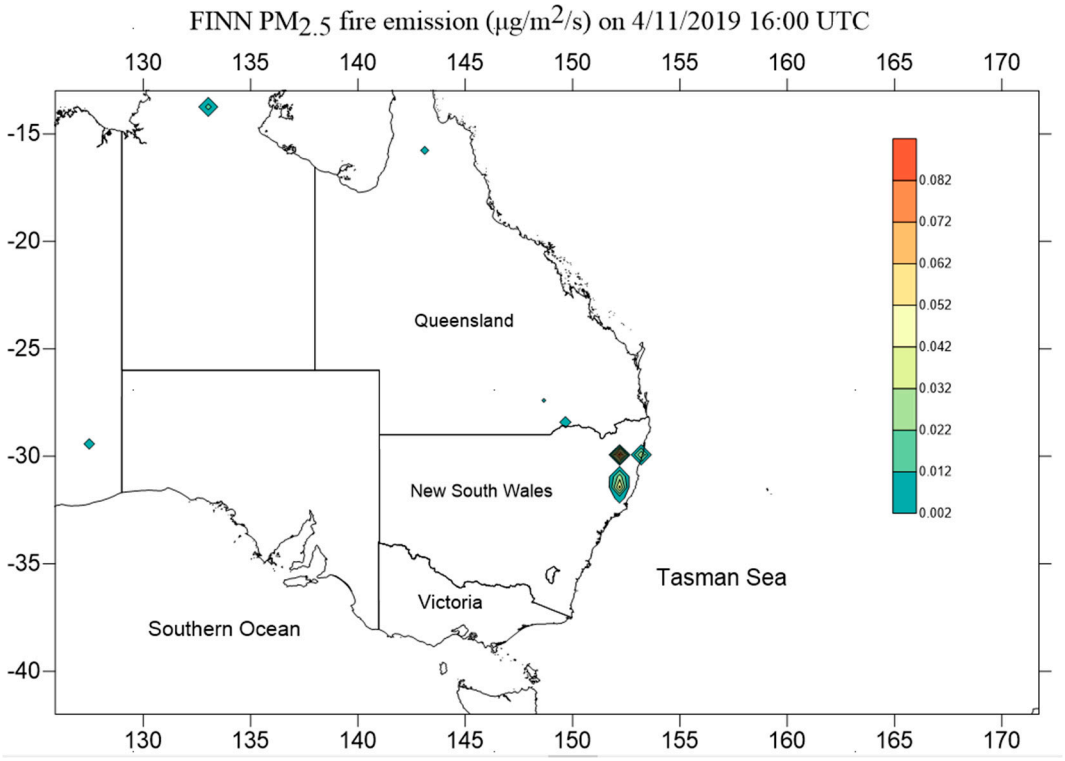

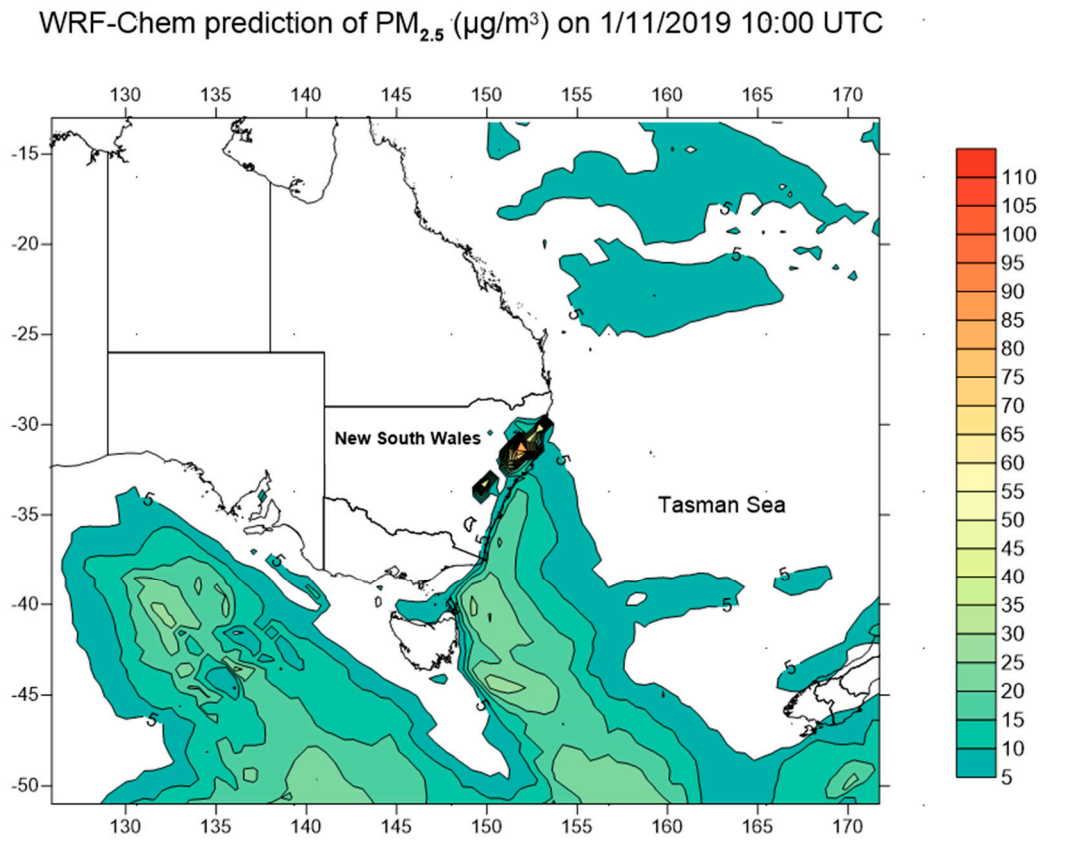

Preprints (www.preprints.org) | NOT PEER-REVIEWED | Posted: 8 January 2024 doi:10.20944/preprints202401.0570.v1

Figure 8. FINN emission of PM2.5 from wildfires in northern New South Wales on 4 November 2019 at 10 UTC (above) and predicted PM2.5 on 1 November 2019 at 10 UTC (below).

Figure 9 shows the predicted deposition velocity on 2 November 2019 was high in the Southern Ocean and in the Pacific Ocean including the Coral Sea, north east of Australia. But ground concentration of $PM_{2.5}$ was low in those area, therefore the deposition rate of $PM_{2.5}$ was not dominant. In contrast, smoke aerosol plumes from the coast of northern NSW to the Tasman Sea and toward south of New Zealand in the Southern Ocean resulted in higher deposition rate o $PM_{2.5}$ and PM_{10} even though the deposition velociy was not high in the Tasman Sea.

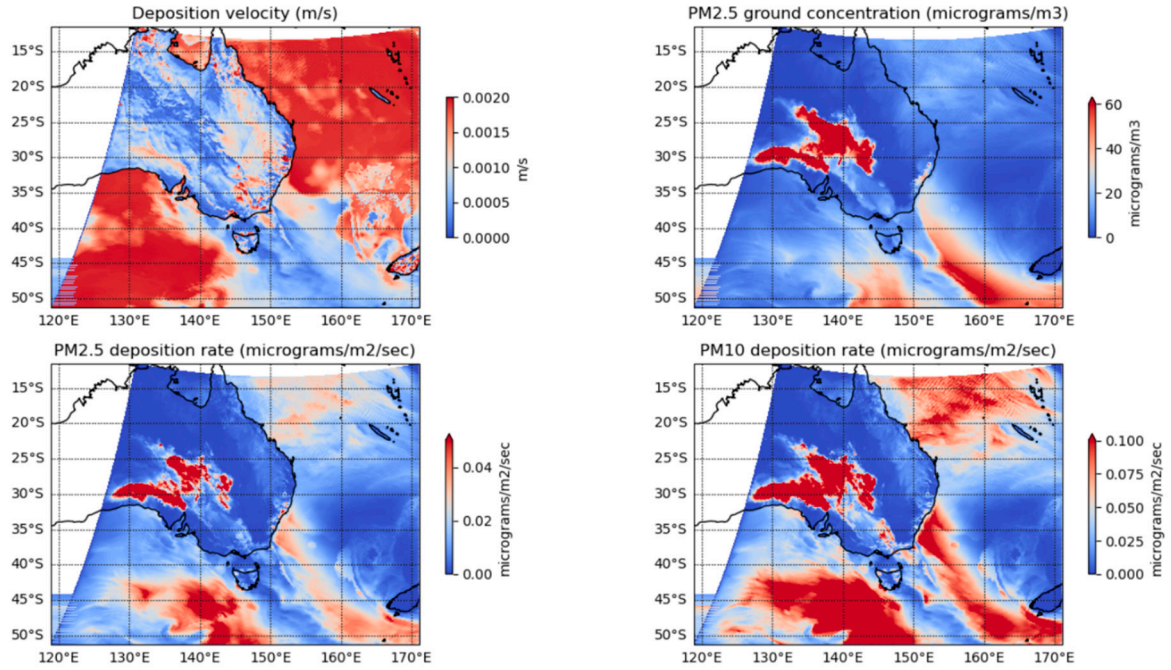

Figure 9. – WRF-Chem prediction of deposition velocity (m/s), $PM_{2.5}$ ground concentration (µg/m3), $PM_{2.5}$ deposition rate (µg/m²/sec) and PM_{10} deposition rate on 2 November 2019 13 UTC.

Figure 10 shows the deposition rate of $PM_{2.5}$ and the wind field at ground level for the subsequent days (3, 5, 6 and 7 November 2019) at various times. The wind field shows northerly wind pushed the smoke plume from the coast in the Tasman Sea to the Southern Ocean south of New Zealand. This smoke plume was then merged with larger plume of sea salt $PM_{2.5}$ arerosols in the Southern Ocean.

Preprints (www.preprints.org) | NOT PEER-REVIEWED | Posted: 8 January 2024 doi:10.20944/preprints202401.0570.v1

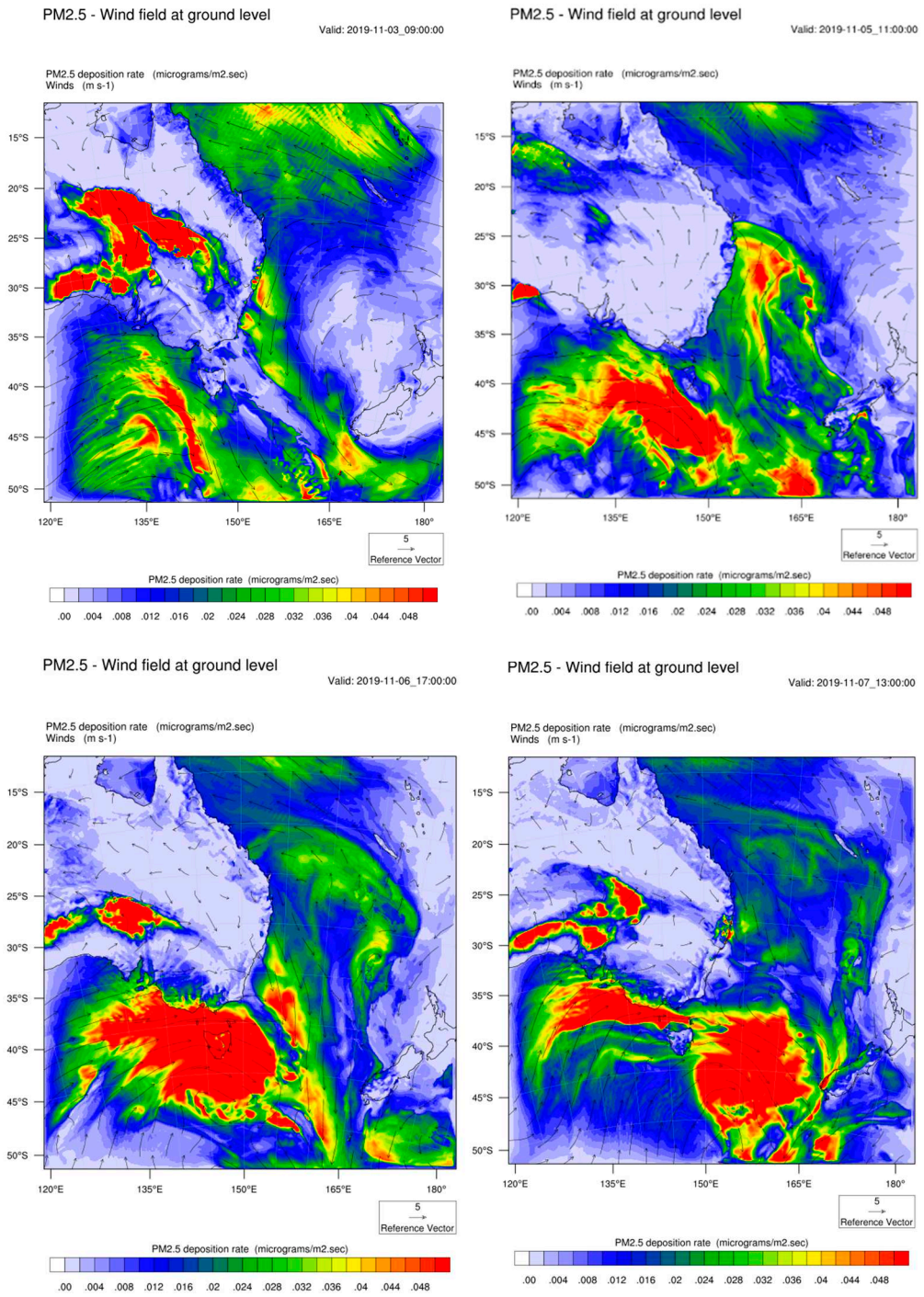

Figure 10. WRF-Chem prediction of $PM_{2.5}$ surface deposition rate (μg/m²/sec) and surface wind field on 3 November 2019 9 UTC, 5 November 2019 11 UTC, 6 November 2019 17 UTC and 7 November 2019 13 UTC .

Figures 9 and 10 show the wildfires in northern NSW in early November resulted in a deposition of smoke aerosols of $PM_{2.5}$ and PM_{10} from 1 to 7 November 2019 mostly in the Southern Ocean south of Tasmania and the Tasmania Sea between Australia and New Zealand.

Similarly to the dust storm analysis of chlorophyll-a, we use the ESA Ocean Color daily chlorophyll-a data at 1km resolution for the period of 1 to 8 December 2019 to correlate with the predicted deposition rate from WRF-Chem simulation. The spatial domain between lat[-24,-50] and lon[142, 179.9], covering the Tasman Sea, is used for the analysis. As chlorophyll-a data is only available at the highest temporal resolution in daily basis, we aggregate hourly deposition data of

Preprints (www.preprints.org) | NOT PEER-REVIEWED | Posted: 8 January 2024 doi:10.20944/preprints202401.0570.v1

PM_{10} and $PM_{2.5}$ into daily data. As $PM_{2.5}$ and PM_{10} prediction from WRF-Chem model are similar in pattern, PM_{10} data analysis is presented here. There are some difficulty in separating PM_{10} from wildfires with other sources such as sea salt which dominates its contribution to PM_{10} in the Southern Ocean. Smoke aerosols and other pollutants from wildfires tend to disperse widely and much faster as compared with dust particles as the buoyant hot plume rise can penetrate the inversion layer in the troposhere. Figure 10 and 11 show the daily deposition rate of PM_{10} and the distribution of daily chlorophyll-a concentrationin the Tasman Sea for 2, 3, 4 and 5 November 2019. The PM_{10} deposition rate clearly shows the plumes of PM_{10} extending from the coast of south eastern Australia to New Zealand for these days.

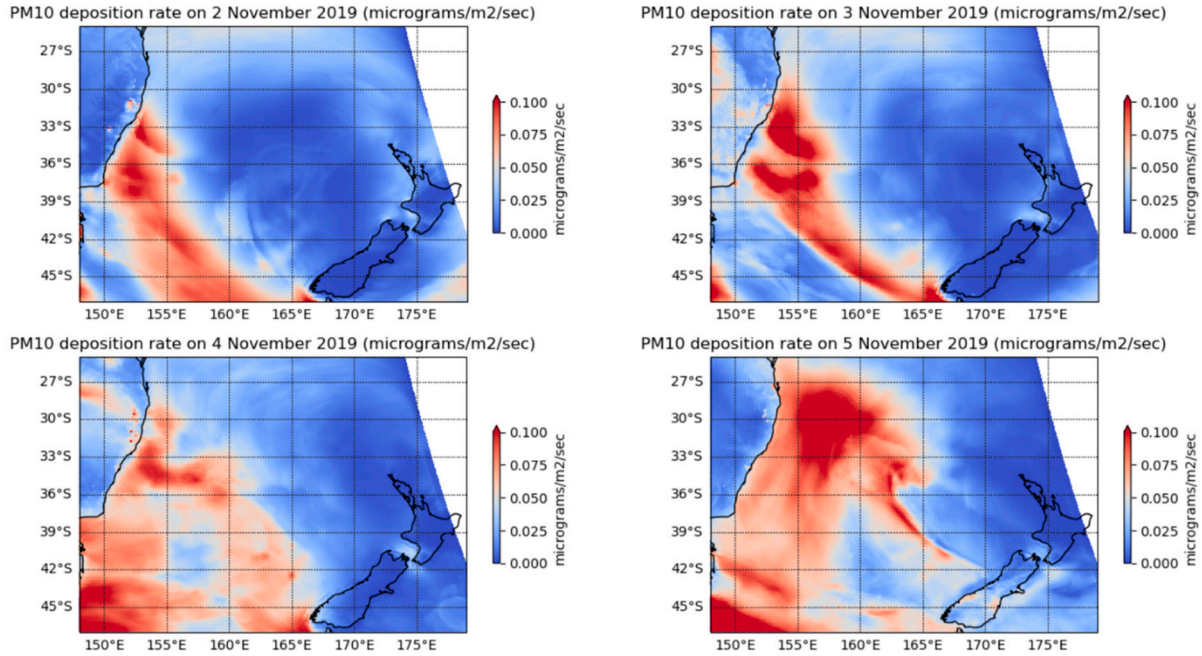

Figure 11. Predicted average PM_{10} deposition rate (μg/m²/sec) in the Tasman Sea on 2, 3, 4 and 5 November 2019.

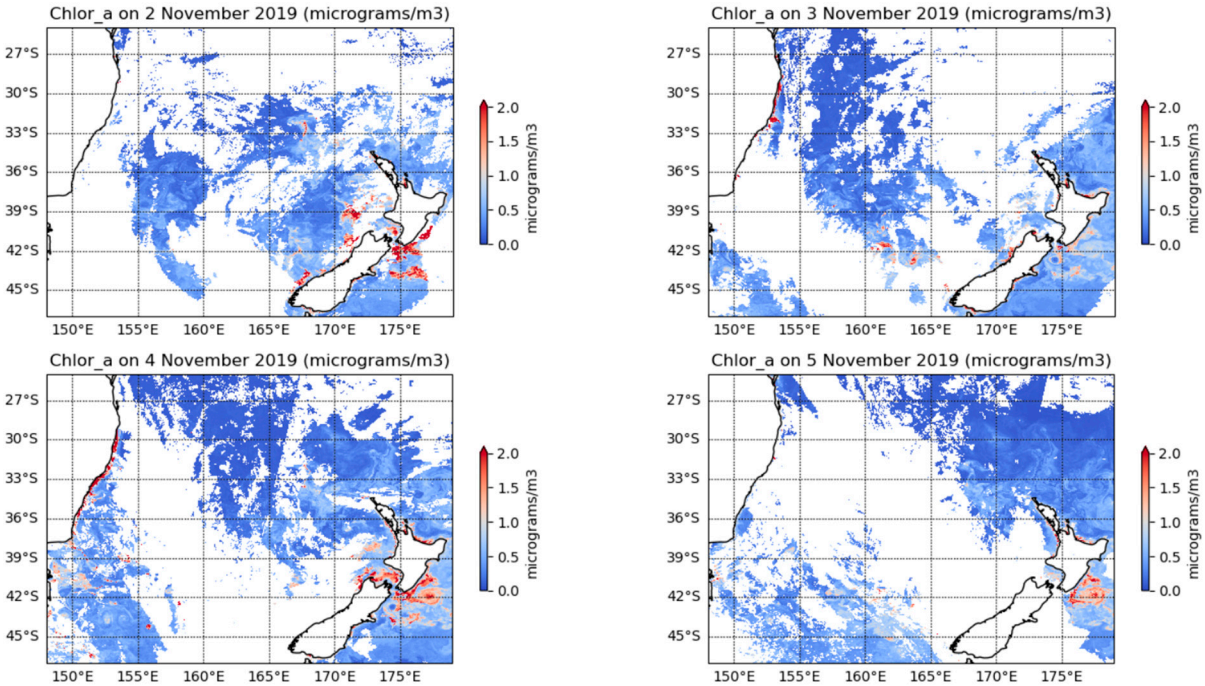

Preprints (www.preprints.org) | NOT PEER-REVIEWED | Posted: 8 January 2024 doi:10.20944/preprints202401.0570.v1

Figure 12. Observed Cholorophyll-a concentration (μg/m^3) in the Tasman Sea on 2, 3, 4 and 5 November 2019.

There are some uncertainties in separating the PM_{10} from wildfires and oathers (mainly sea salt emission from the ocean). The Southern Ocean emits significant amount of sea salt as shown in the predicted PM_{10} in this ocean south of the Australian continent and the Tasman Sea. This is different from the dust strom case. In the dust storm simulation, the total dust consisting of particles of different sizes (0.2 - 20 μm) is predicted separately from other sources so there are no ambiguity in assesing or correlating its impact on photoplankton growth. The PM_{10} plumes not far from wildfire sources allows one to be certain of their sources. Near the coast of New South Wales, close to the wildfire sources, the high concentration of chlorophyll-a concentration is observed such as in Figure 13.

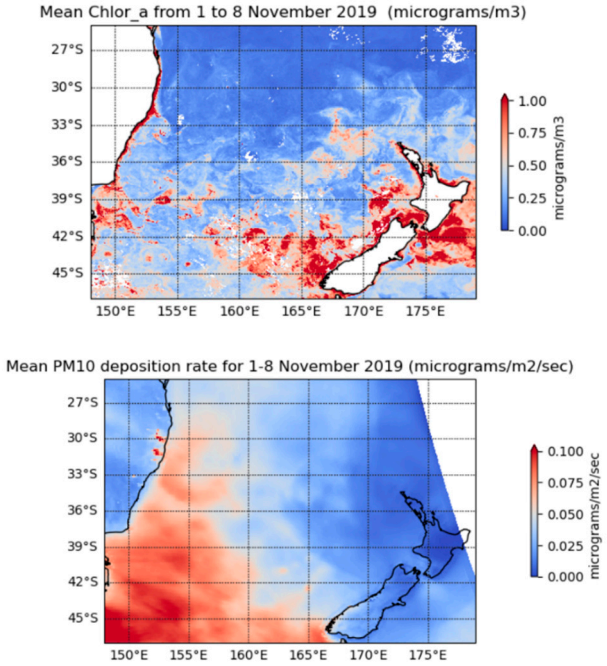

Figure 13. Mean of Chlorophyll-a concentration (left) and mean of PM_{10} deposition rate (right) from 1 to 8 of November 2019 in the Tasman Sea.

Figure 14 shows the time series of chlorophyll-a daily concentration and PM10 deposition rate at 5 point locations in the sea off the coast of northern NSW. High concentration of chlorophyll_a occurred on the 4 and 6 of November 2019 but time series (hourly) of predicted PM10 deposition rate at 5 point locations have high deposition rates occurred on 3 and 5 November 2019. On the 7 and 8 of November 2019, high PM_{10} deposition rates occurred but there no chlorophyll-a measurments due to cloud coverage of the area.

Other air quality model such as WRF-CMAQ allows one to tag the sources and therefore can determine separately its contribution to the total load of predicted pollutant concentration. However, WRF-CMAQ is more complex to use in this mode and requires extensive computing resources. Other source of uncentainty in accessing the association of particulate matters deposition such as some aerosols in the ocean and phytoplankton growth is the growth of phytoplankton also depends on a number of factors, such as macronutrient levels, seasonal timing, light condition, and the initial state of the water ecosystem [19].

Preprints (www.preprints.org) | NOT PEER-REVIEWED | Posted: 8 January 2024 doi:10.20944/preprints202401.0570.v1

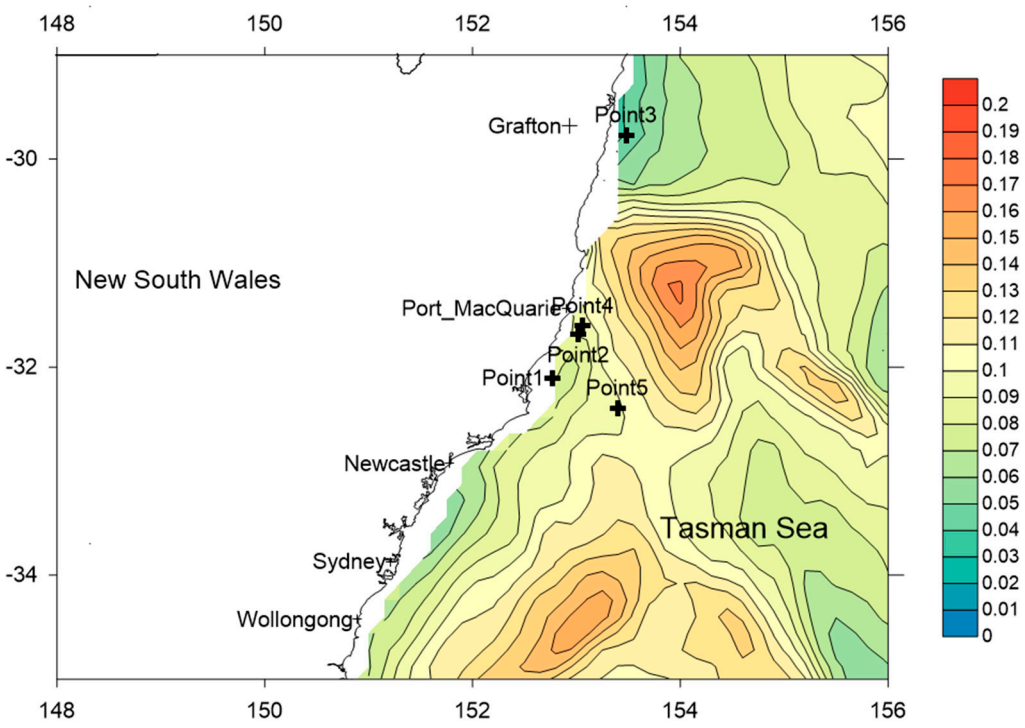

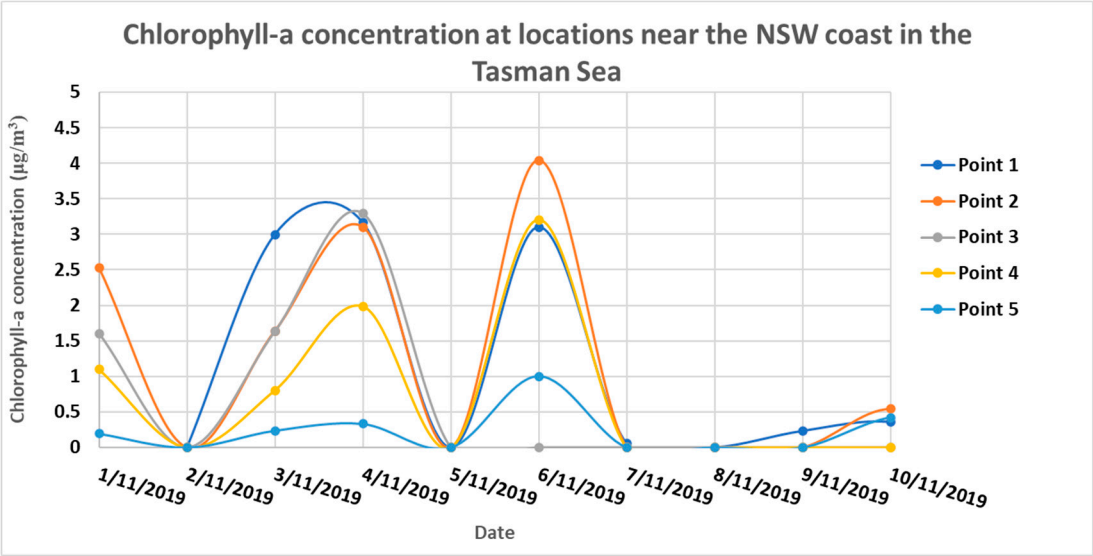

Preprints (www.preprints.org) | NOT PEER-REVIEWED | Posted: 8 January 2024 doi:10.20944/preprints202401.0570.v1

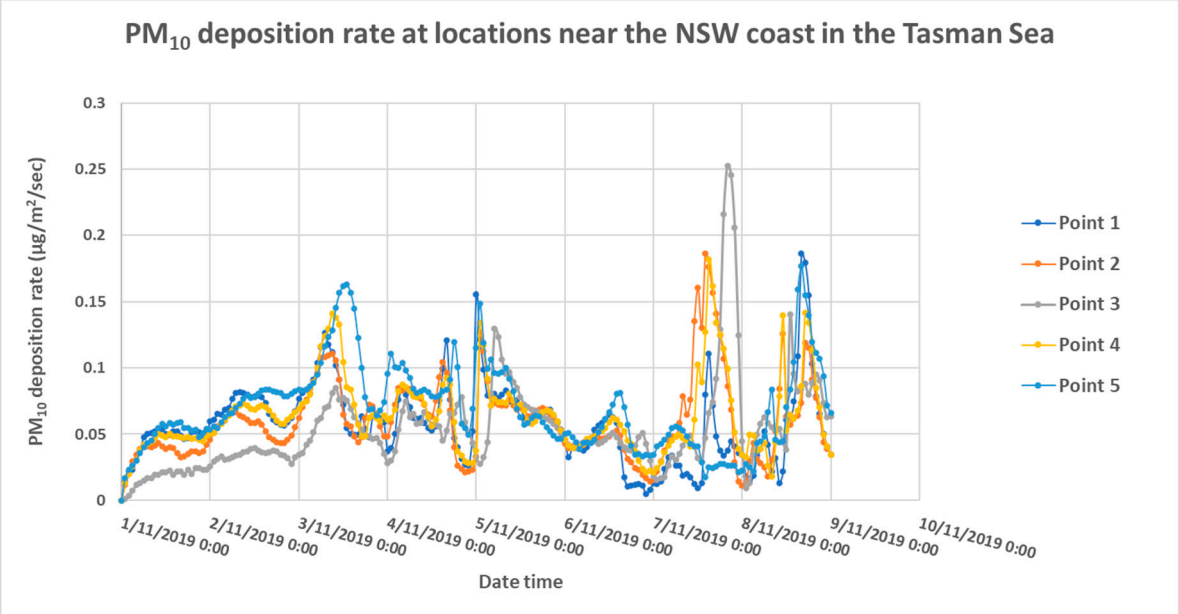

Figure 14. PM_{10} deposition rate (µg/m3) contour over the ocean on 4 November 2019 04 UTC and 5 point locations (a). Time series of chlorophyll-a concentration (µg/m^3) at 5 point locations along the coast of NSW from 1 to 10 November 2019 (b) where high concentration occurred on the 4 and 6 of November 2019. Time series (hourly) of predicted PM_{10} deposition rate at 5 point locations (c) where high deposition rates occurred on 3 and 5 November 2019. Coordinates of the point locations: Point 1 (152.771, -32.1042), Point 2 (153.021, -31.6875), Point 3 (153.479, -29.77), Point 4 (153.062,-31.6042), and Point 5 (153.396,-32.3958).

From the WRF-Chem simulation, the total deposition of PM_{10} and $PM_{2.5}$ in the Tasman Sea for the period of 1 to 8 November 2019 (the first stage of the Black Summer wildfires of 2019-2020) is approximately 132,000 tons and 45,400 tons respectively. For deposition on land, the figures are 151,000 tons and 34,000 tons respectively.

3.3. Comparision of the dust storm impact and the wildfire impact on phytoplankton growth

WRF-Chem model was used with AFWA-GOCART dust emission scheme for the dust storm while the same model configuration but with MOZART chemistry mechanism and FINN (Fire Emission Inventory for NCAR) emission was used for wildfire simulation. For the Black Summer megafires lasting from November 2019 to January 2020, the peak of phytoplankton blooms occurred from January to early March 2020 when deposition of smoke aerosols on the ground from aerosols above in the troposphere and in higher layers happened after they were being transported higher and farther away from sources. After this time from March, the growth disappeared indicating that some of the carbon emitted by the megafires was reabsorbed by the ocean.

In comparison with the effect of the February 2019 dust storm on phytoplankton growth shown in Figure A2(g), the dust storm emitted much less carbon and its effect on phytoplankton growth is via iron (Fe) content in the dust. From these observations it can be inferred that the dust storms typically contribute to net carbon uptake and export carbon to the deeper layers of the ocean, acting as a sink. Conversely, the wildfires emit carbon to the atmosphere, some of which is reabsorbed by vegetation on land and phtytoplankton in the ocean. The wildfire events cause carbon loss to the atmosphere or at best carbon neutral when reabsortion by biomass on land and ocean occurs. The amount of PM_{10} aerosols deposited in the Tasman Sea for the period 1 to 8 November 2019 from the wildfires (132,000 tons) is much larger than that of total dust deposit (1230 tons) due to the dust storm from 11 to 15 February 2019.

 doi:10.20944/preprints202401.0570.v1

3.3. Discussion

In this paper, a comparison study of the effect of dust storms and wildfires on phytoplankton growth in Tasman Sea and Southern Ocean was conducted, investigating the 14 to 16 February 2019 dust storm and the first stage (1-8 November 2019) of the Black Summer megafires (November 2019-January 2020) as case studies. Both events promoted phytoplankton growth but the megafires triggered a massive growth all around the southern hemisphere. The difference can be attributed to 2 factors: firstly, the megafires were much bigger and longer and secondly, the emitted carbonaceous nutrients from the fires deposited on water surface can promote stronger growth. The total emission of carbon from the megafires was estimated by various authors [29] [26] as ~0.7 Pg (petagrams C) which is about 5 times the total annual Australian anthropogenic emission. Figure 5 shows the anomaly of chlorophyll-a concentration in January, February and March 2020 from average of the same period 2002-2010.

Bowman et al. 2020 [34] in their study of Australian forests and megafires have highlighted the risk of dwindling carbon stocks from more frequent fires due to climate change. The increasing megafires frequencies will reduce the recovery capacity of reabsorbing the emitted CO_2 from the eucalyptus forest even though such native eucalyptus forests are known to be resilient and highly adaptable to fire-induced environment on the dry Australian continent. It is assumed by many policy makers that rapid recovery by forest generation would therefore result in CO_2 emissions to be reabsorbed and fixed in those carbon storage sites [35]. However, rapid climate change could have run-away positive feedback that will leave no time for forest recovery and CO_2 reabsorption due to the anticipated increase in the frequency magnitude of wildfires in Australia. It was suggested by Vajda et al. 2020 [36] in their sedimentary study in the Sydney basin that the End-Permian mass extinction event (EPE) about 252 million years ago was due to the deforestation, wildfires and flooding.

In the Bowman et al. 2020 [34] study of carbon emission from the 2019-2020 wildfires, they estimated that about 0.67 Pg (Petagrams, 1 Pg is 10^{15} grams) of carbon emitted from the 2019-2020 wildfires. This can be compared with the global 2019 annual emission of fossil fuel and land use change (mainly deforestation) of about 9.9 Pg and 1.8 Pg of carbon respectively [37]. Van der Velde et al., 2021 [26] subsequently estimated about 0.715 Pg of carbon emitted from this wildfires period from November 2019 to January 2020, exceeding Australia's 2018 anthropogenic CO_2 emissions of 537.4 million tonnes (0.147 Pg C) [19]. The emission of carbon from this 2019-2020 wildfires is nearly 5 times the total annual Australian anthropogenic carbon emission.

However, the effect of wildfires such as the megafires of 2019-2020 on promoting phytoplankton growth in the Southern Ocean can have a potential to offset the emitted CO_2 significantly. Tang et al. 2021[19], showed that the satellite-estimated marine net primary production (NPP) and export production (EP) increased substantially during the 2019–2020 wildfire period compared with the monthly climatologies. From October 2019 to April 2020, a cumulative net additional uptake of ~186 ± 90 Tg (Teragrams or 10^{12} grams) of carbon was absorbed by phytoplankton blooms which is equivalent to ~95 ± 46% of the CO_2 emission (~195 Tg C) from the 2019–2020 Australian wildfires. Even though their estimate of 0.195 Pg carbon emission from the 2019-2020 wildfires is lower than those from Bowman et al. 2020 [34] (0.67 Pg) and from Van der Velde et al, 2021 [26] (0.715 Pg), but the high proportion of carbon uptake by phytoplankton growth showed that most of the emitted carbon by the wildfires was absorbed via phytoplankton growth in the Southern Ocean.

As Tang et al. 2021 [19] noted that in their study, not all bodies of oceanic water respond to Fe-fertilisation by pyrogenic aerosols with strong phytoplankton growth as this also depends on the macronutrient levels, seasonal timing, light condition, and the initial state of the water ecosystem. Such is the case of oligotrophic subtropical waters east of Australia where limit of macronutrient level show lack of chlorophyll-a response.

As large wildfires occur less frequent compared to dust storms over the southern part of the Australian continent, and the Australian soil contains more Fe than that in biomass, the phytoplankton bloom in the seas off the south-eastern Australian coast from dust is more significant.

 doi:10.20944/preprints202401.0570.v1

Even though air quality model is a useful tool in estimating the dispersion, transport and deposition of pollutants from source emission, there are some uncertainties in the modelling results. Tan et al. 2019 in their study of difference in prediction of particulate matter (PM) among various models including WRF-CMAQ (v4.7.1 and v5.0.2), WRF-Chem (v3.6.1 and v3.7.1), GEOS-Chem, NHM27 Chem, NAQPMS and NU-WRF, have found that the difference is mainly due to different natural emission mechanism such as dust and sea salt, in initial and boundary conditions, in gas-particle conversion phase and in different amounts of depositions.

Zhang et al. (2019) [38] compared the modelled dust deposition using the GOCART aerosol scheme in WRF-Chem with observed dust deposition and found that modelled dust deposition is highly underestimated by more than one order of magnitude compared to the observed deposition. This indicates that the dry deposition scheme [32] in GOCART aerosol scheme may not be suitable for dust simulation and needs to be further improved. The Ginoux DSF used in WRF-Chem is a static function as it is based on topography. This can be modified to account for the changing land cover. Besides improving the DSF, other aspects of dust emission processes can be improved to characterise the emission over surface roughness such as [39] who proposed using albedo from satellites to better represent shadow and sheltered area from dust mobilisation.

If both wildfire and dust storm event happen at the same time such as the dust storm event in east coast Australia in February 2019 with wildfires happened at the same time in northern NSW. How do we separate the dust and fire carbon impacts? This is difficult to work out if both events happened at the same time which can happen frequenly in the futre changing climate. Modelling is one of the answers in this case.

In this study, we have shown that there is strong evidence that the sequestration of CO_2 by enhanced biological pump via phytoplankton growth occurred during the February 2019 dust storm and the Black Summer 2019/2019 wildfires events. But how long this sequestration and what amount of carbon would store in the ocean at different depth is not known and will be the subject for further study. This is important for policy makers wanting to account for the carbon absorbed and sequestered in the ocean to formulate response to climate change.

4. Conclusion

In this study, we have chosen the February 12-16 2019 dust storm and the megafires in November to January 2019-2020 for comparison of phytoplankton growth in the Tasman Sea as case studies. We have shown that there is a strong evidence from simulation study that the growth in phytoplankton in the Tasman Sea in mid-February 2019 and in the early stage of the Black Summer wildfires (from 1 to 8 November 2019) was due to the dust deposition from the dust storm and the smoke aerosols from the wildfires respectively. The amount of deposition of particulate matter from the wildfires is much larger than that of the dust storm. The WRF-Chem air quality model has been shown to be an useful tool to study and determine the patern of impact of pariculate matter on the phytoplankton growth in the Tasman Sea.

The phytoplankton growth absorbed CO_2 via photosynthesis and hence acted as carbon sink. Both events promoted phytoplankton growth but the megafires triggered a massive growth all around the southern hemisphere. The difference can be attributed to two factors: firstly, the megafires were much larger and longer and secondly, the emitted carbonaceous nutrients from the fires deposited on water surface can promote stronger growth of phytoplankton.

The phytoplankton blooms occurred from December 2019 to early March 2020, shortly following the wildfire events. After that the growth disappeared and is largely attributed to being reabsorbed by the ocean. How long and how much of that carbon was sequestered at different depth in the Tasman and Southern Oceans is not known and requires further study.

Author Contributions: Conceptualization, H.D.N., M.A., J.L, M.R. ; methodology, H.D.N., S.W.; data procurement, D.S., T.T., K.M., X.B., D.F. and H.N.; formal analysis, H.D.N.; investigation, H.D.N., F.J., L.T.-C.C., ; writing—original draft preparation, H.D.N., J.F.; software, D.F.; visualization, H.D.N.; supervision, H.D.N.,

 doi:10.20944/preprints202401.0570.v1

M.A. and M.R.; and project administration, H.D.N., M.A. and M.R.. All authors have read and agreed to the published version of the manuscript.

Funding: This research received no external funding.

Institutional Review Board Statement: Not applicable.

Informed Consent Statement: Not applicable.

Data availability statement: Data available upon request to the corresponding author

Acknowledgement: The following data sources are gratefully acknowledged: FINN fire emission datasets from the NCAR, US (Available online: http://www.acom.ucar.edu/acresp/MODELING/finn_emis_txt/. accessed on 27 March 2021), MODIS Aqua/Terra satellite hot spots data from the NASA, US, final analysis (FNL) reanalysis data from the National Center for Environmental Prediction (NCEP), US. Research product of aerosol properties and chlorophyll-a (produced from Himawari-8) was provided by the P-Tree System, Japan Aerospace Exploration Agency (JAXA). Time series of chlorophyll-a 1-day, 8-day data was obtained from Ocean Colour – Climate Change Initiative with support from the European Space Agency.

Conflicts of Interest: The authors declare no conflict of interest.

Appendix A

The WRF-Chem simulation from 11 to 16 February 2019 of the February 2019 dust storm as shown in Figure A1 below shows the progress of the dust storm from Central Australia to Northern Australia, Western Australia and the eastern states of Austrlia to the Tasman Sea.

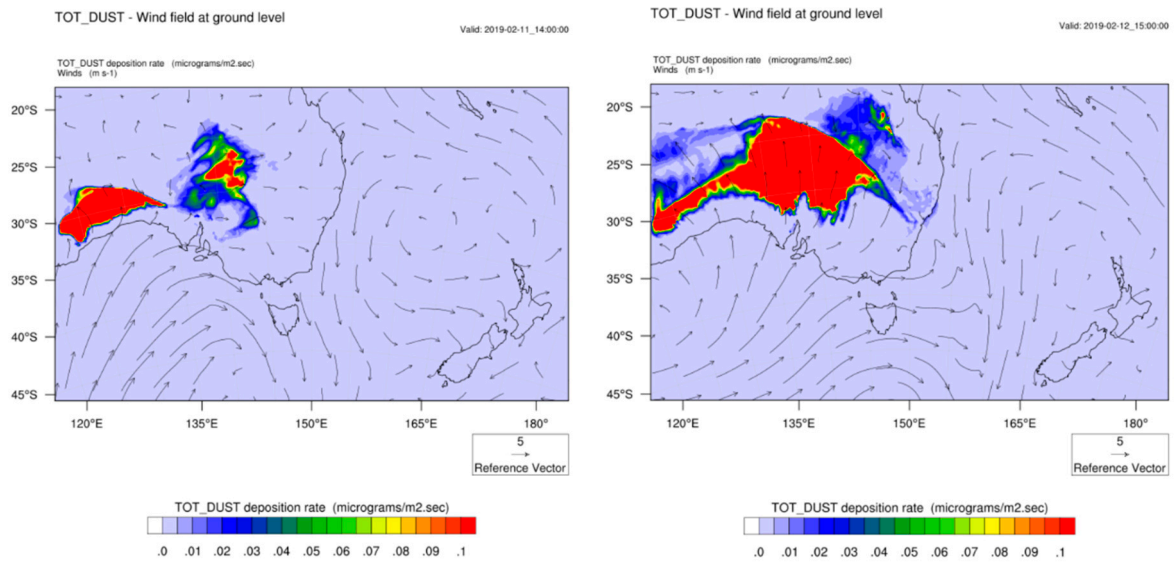

Preprints (www.preprints.org) | NOT PEER-REVIEWED | Posted: 8 January 2024 doi:10.20944/preprints202401.0570.v1

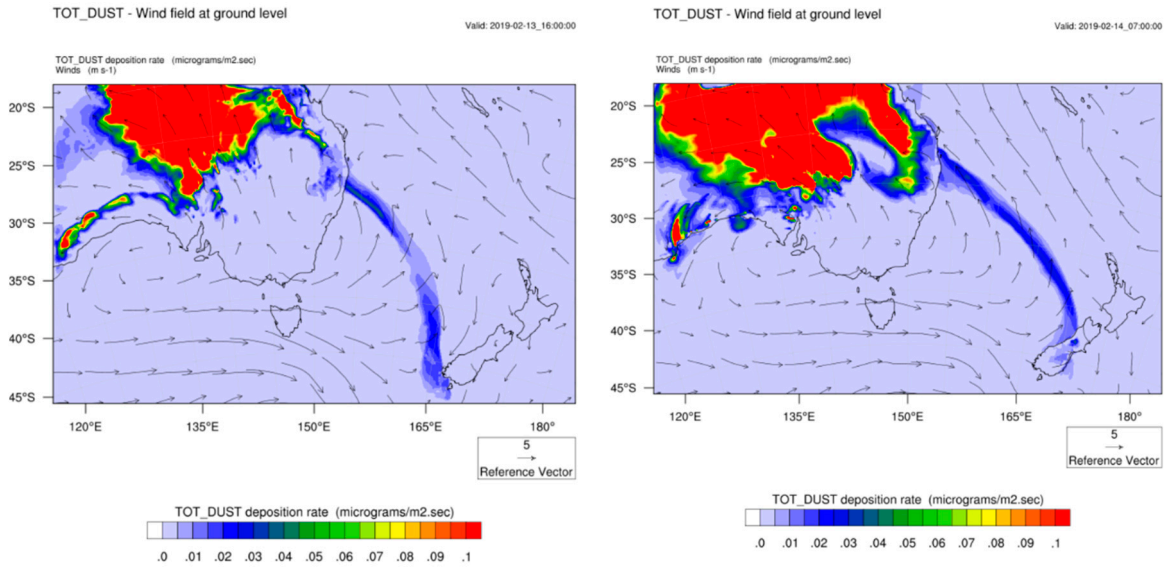

Figure A1. Progress of the dust storm from 12 to 16 February 2019 as simulated by WRF-Chem air quality model for the period 11 to 16 February 2019. Total dust deposition rate (μg/m^3/sec) at 11 February 2019 14:00 UTC, 12 February 2019 15:00 UTC, 13 February 2019 16:00 UTC and 14 February 201907:00 UTC.

Appendix B

Himawarri geostationary satellite from the Japan Aerospace Exploration Agency over the Pacific Ocean also measures the AOD and chlorophyll-a concentration. For the period of dust storm in February 2019, the AOD and chlorophyll-a concentration for 14 and 15 February 2019 are obtained and shown in Figure A.2 below. The data from the Himawarri satellite corresponds well with that of NASA MODIS Aqua/Terra sattelite measurements.

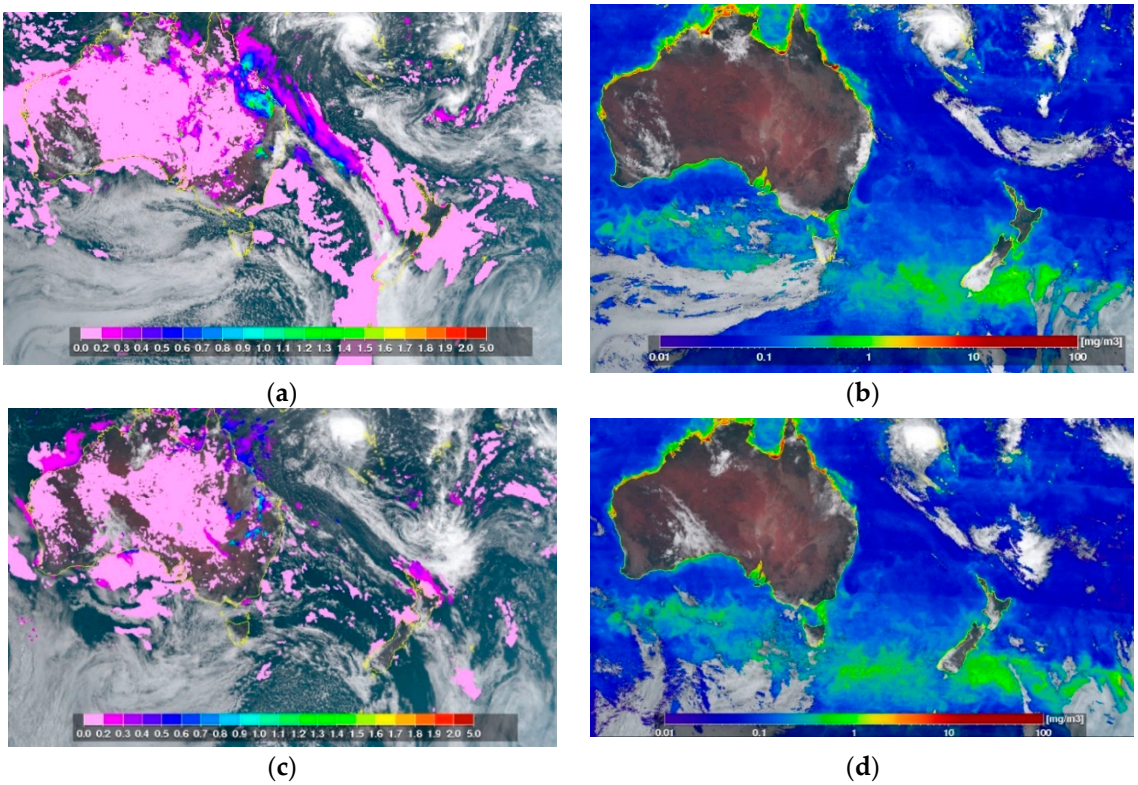

(**a**) (**b**)

(**c**) (**d**)

Preprints (www.preprints.org) | NOT PEER-REVIEWED | Posted: 8 January 2024 doi:10.20944/preprints202401.0570.v1

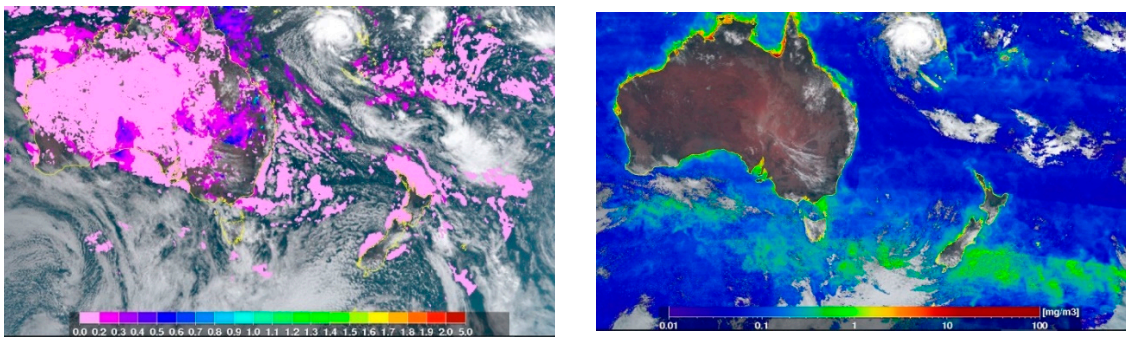

(e) (f)

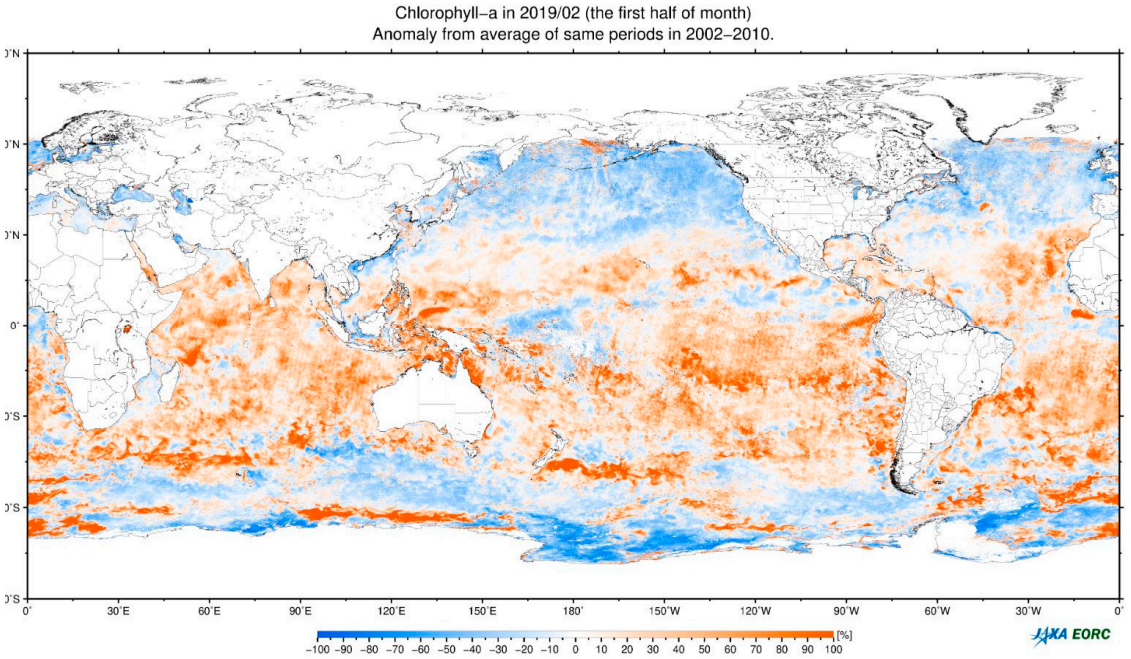

(g)

FigureA2. – Daily AOD and chlorophyll-a concentration on 14 February 2019 (a) (b), 15 February 2019 (c) (d) and 16 February 2019 (e) (f) as detected by Himawarri geostationary satellite (source: Japan Aerospace Exploration Agency, https://www.eorc.jaxa.jp/ptree/). And anomaly of chlorophyll-a concentration in first half of February 2019 from average period 2002-2010 after the dust storm (g).

Appendix C

The monthly average chlorophyll-a concentration as detected by Himawarri sensor in December 2019 and January 2020 shows an increase in clhorophyll-a concentration compared to the monthly average of the previous year.

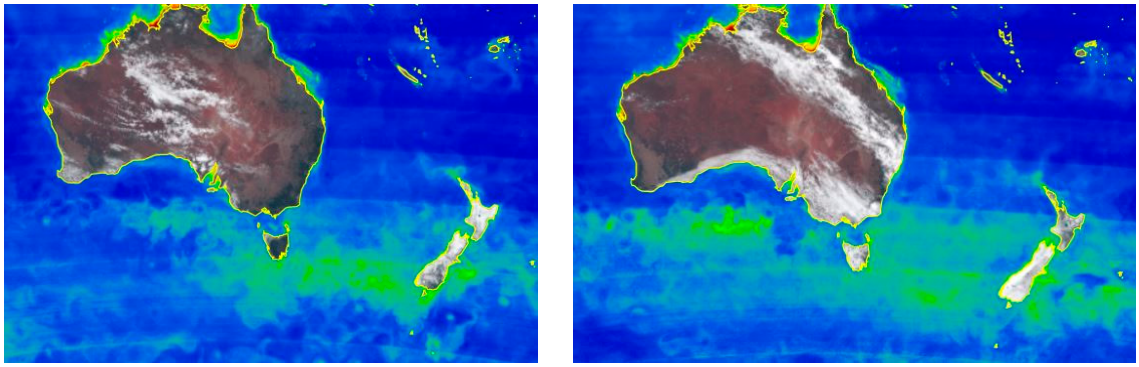

(a) (b)

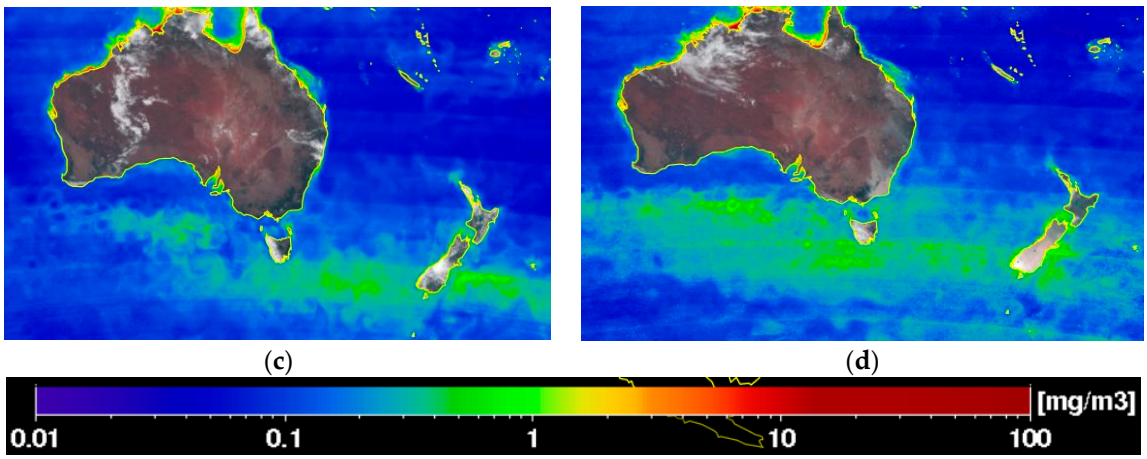

Figure A3. Monthly concentration of chlorophyll-a in December 2018 (a) as compared to that in December 2019 (b) and chlorophyll-a concentration (mg/m^3) in January 2019 (c) as compared to that in January 2020 (d).

References

1. Boyd, P., Jickells, T., Law, C., Blain, S., et. al., 2007, Mesoscale iron enrichment experiments 1993–2005: Synthesis and future directions. *Science* 315, 612–617, DOI: 10.1126/science.1131669
2. Boyd, P.W., McTainsh, G., Sherlock, V., Richardson, K., Nichol, S., Ellwood, M., Frew, R., 2004. Episodic enhancement of phytoplankton stocks in New Zealand subantarctic waters: Contribution of atmospheric and oceanic iron supply. *Global Biogeochemical Cycles* 18.
3. Earthdata Search: MODISA_L2_OC; OceanColor Web - Level 1&2 Browsers; OceanColor Web - Chlorophyll a; NASA Earth Observations - Chlorophyll Concentration
4. Hoffmann, L., Peeken, I., Lochte, K., Assmy, P., Veldhuis, M., 2006, Different reactions of Southern Ocean phytoplankton size classes to iron fertilization, Limnol. Oceanogr.,51(3), 2006, 1217–1229
5. Gregg, W., Rousseaux, C., 2019, Global ocean primary production trends in the modern ocean color satellite record (1998–2015), *Environ. Res. Lett.*, 14 124011
6. Calvo, E., Pelejero, C., Logan, G., De Deckker, P., 2004. Dust-induced changes in phytoplankton composition in the Tasman Sea during the last four glacial cycles. *Paleoceanography* 19, 10.1029/2003PA000992.
7. Smetacek, V., Klaas, C., Strass, V., et al. 2012, Deep Carbon Export from a Southern Ocean Iron-fertilized Diatom Bloom, *Nature* 487(7407):313-9, DOI: 10.1038/nature11229
8. Smetacek, V., Naqvi, S., 2008, The next generation of iron fertilization experiments in the Southern OceanPhil. , Trans. R. Soc. A.3663947–3967, http://doi.org/10.1098/rsta.2008.0144
9. Martínez-García, A., Sigman, D.M., Ren, H., Anderson, R.F., Straub, M., Hodell, D.A., Jaccard, S.L., Eglinton, T.I. and Haug, G.H., 2014. Iron fertilization of the Subantarctic Ocean during the last ice age. *Science*, 343(6177), pp.1347-1350.
10. Ronge, T., Frische, M., Fietzke, J. et al., 2021, Southern Ocean contribution to both steps in deglacial atmospheric CO2 rise. *Scientific Reports*, 11, 22117, https://doi.org/10.1038/s41598-021-01657-w
11. Siegell, D., DeVries, T., Doney, S., Bell, T., 2021, Assessing the sequestration time scales of some ocean-based carbon dioxide reduction strategies, *Environ. Res. Lett.* 16 (2021) 104003, https://doi.org/10.1088/1748-9326/ac0be0
12. Rodríguez, S., Prospero, J., Lopez-Darias, J., García-Alvarez, M. et al., 2021, Tracking the changes of iron solubility and air pollutants traces as African dust transits the Atlantic in the Saharan dust outbreaks, *Atmospheric Environment* (1967), DOI: 10.1016/j.atmosenv.2020.118092
13. Lauderdale, J., Braakman, R., Forget, G., Dutkiewicz, S., Follows, M., 2020, Microbial feedbacks optimize ocean iron availability. *Proceedings of the National Academy of Sciences*, 201917277. doi:10.1073/pnas.1917277117
14. Perron, M., Proemse, B., Strzelec, M., Gault-Ringold, M., Boyd, P. et al., 2020, Origin, transport and deposition of aerosol iron to Australian coastal waters, *Atmospheric Environment*, 228:117432, https://doi.org/10.1016/j.atmosenv.2020.117432
15. Gabric, A.J., Cropp, R., McTainsh, G., Butler, H., Johnston, B.M., O'Loingsigh, T., Van Tran, D., 2015. Tasman Sea biological response to dust storm events during the austral spring of 2009. Marine and *Freshwater Research* 67, 1090-1102., https://doi.org/10.1071/MF14321

16. Gabric, A.J., Cropp, R.A., McTainsh, G.H., Johnston, B.M., Butler, H., Tilbrook, B., Keywood, M., 2010. Australian dust storms in 2002-2003 and their impact on Southern Ocean biogeochemistry. *Global Biogeochemical Cycles* 24., https://doi-org.virtual.anu.edu.au/10.1029/2009GB003541
17. Nguyen, H., Riley, M., Leys, J., Salter, D., 2019, Dust Storm Event of February 2019 in Central and East Coast of Australia and Evidence of Long-Range Transport to New Zealand and Antarctica. *Atmosphere* 2019, 10, 653. https://doi.org/10.3390/atmos10110653
18. Hamilton, D., Scanza, R., Rathod, S., et al. 2020, Recent (1980 to 2015) Trends and Variability in Daily-to-Interannual Soluble Iron Deposition from Dust, Fire, and Anthropogenic Sources, *Geophysical Research Letters*, 47(17), DOI: 10.1029/2020GL089688
19. Tang, W., Llort, J., Weis, J., Perron, M., Basart, S., et al., 2021, Widespread phytoplankton blooms triggered by 2019–2020 Australian wildfires, *Nature* 597, 370–375 (2021). https://doi.org/10.1038/s41586-021-03805-8
20. Nguyen, H.D, Azzi, M., White, S., Salter, D., Trieu, T., Morgan, G., ẹt. al., 2021, The Summer 2019-2020 Wildfires in East Coast Australia and Their Impacts on Air Quality and Health in New South Wales, Australia. *Int J Environ Res Public Health*. ;18(7):3538. doi: 10.3390/ijerph18073538. PMID: 33805472; PMCID: PMC8038035.
21. Davey, S.A., Sarre, A., 2020, Editorial: The 2019/20 Black Summer bushfires, *Aust. For.* 2020, 83, 47–51, doi:10.1080/00049158.2020.1769899
22. Australian Institute of Health and Welfare (AIHW). Australian Bushfires 2019–20, Exploring the Short-Term Health Impacts, 2020. Available online: https://www.aihw.gov.au/getmedia/a14c3205-784c-4d81-ab49-a33ed4d3d813/aihw-phe-276.pdf.aspx?inline=true (accessed on 14 May 2023).
23. ECMWF (European Centre for Medium-Range Weather Forecasts). Copernicus Atmosphere Monitoring Service: Wildfires continue to rage in Australia. Reading, United Kingdom: ECMWF. 2020. Available online: https://atmosphere.copernicus.eu/wildfires-continue-rage-australia (accessed on 14 May 2023).
24. Fasullo, J., Rosenbloom, N., Buchholz, R., 2023, A multiyear tropical Pacific cooling response to recent Australian wildfires in CESM2, *Sci. Adv*. 9, eadg1213 (2023)
25. Qiao, X., Tang, Y., Hu, J., Zhang, S., et al., 2015, Modeling dry and wet deposition of sulfate, nitrate, and ammonium ions in Jiuzhaigou National Nature Reserve, China using a source-oriented CMAQ model: Part I. Base case model results, *Sci Total Environ.*, 532:831-9. doi: 10.1016/j.scitotenv.2015.05.108.
26. van der Velde, I., van der Werf, G., Houweling, S. et al., 2021, Vast CO2 release from Australian fires in 2019–2020 constrained by satellite, *Nature* 597, 366–369 (2021). https://doi.org/10.1038/s41586-021-03712-y
27. Foroushani, M., Opp, C., Groll., M., Nikfal, A., 2020, Evaluation of WRF-Chem Predictions for Dust Deposition in Southwestern Iran, *Atmosphere*, 11(7), 757; https://doi.org/10.3390/atmos11070757
28. Zhang, X., Sharratt, B., Liu, L., Wang, Z., Pan, X., et al., 2018, East Asian dust storm in May 2017: observations, modelling and its influence on Asia-Pacific region, *Atmos. Chem. Phys. Discuss.*, https://doi.org/10.5194/acp-2018-205.
29. Ginoux, P., Chin, M., Tegen, I., Prospero, J.M., Holben, B., Dubovik, O. and Lin, S.J., 2001. Sources and distributions of dust aerosols simulated with the GOCART model, *Journal of Geophysical Research: Atmospheres*, 106(D17), pp.20255-20273.
30. Parajuli, S., Zender, C., 2017, Connecting geomorphology to dust emission through high-resolution mapping of global land cover and sediment supply, *Aeolian Research*, 27: 47-65, https://doi.org/10.1016/j.aeolia.2017.06.002
31. Ukhov, A., Ahmadov, R., Grell, G., Stenchikov, G., 2021, Improving dust simulations in WRF-Chem v4.1.3 coupled with the GOCART aerosol module, *Geosci. Model Dev.*, 14, 473–493, 2021, https://doi.org/10.5194/gmd-14-473-2021
32. M.L. Wesely, M., 1989, Parameterization of surface resistances to gaseous dry deposition in regional-scale numerical models. *Atmospheric Environment* (1967), 23:6,
33. Shaw, E.C., Gabric, A.J., McTainsh, G.H., 2008. Impacts of aeolian dust deposition on phytoplankton dynamics in Queensland coastal waters. *Marine and Freshwater Research* 59, 951-962.
34. Bowman, D., Williamson, G., Price, O., et al., 2020, Australian forests, megafires and the risk of dwindling carbon stocks, *Plant Cell Environ.*, 44, 347–355, https://doi.org/10.1111/pce.13916
35. Kashian, D., Romme, W., Tinker, D., Turner, M., Ryan, M., 2006, Carbon Storage on Landscapes with Stand-replacing Fires, *BioScience*, 56:7, 598–606, https://doi.org/10.1641/0006-3568(2006)56[598:CSOLWS]2.0.CO;2
36. Vajda, V., McLoughlin, S., Mays. C., Frank, T., et al. 2020, End-Permian (252 Mya) deforestation, wildfires and flooding—An ancient biotic crisis with lessons for the present, Earth and Planetary Science Letters, 529:115875, https://doi.org/10.1016/j.epsl.2019.115875
37. Friedlingstein, P., O'Sullivan, M., Jones, M., et. al., 2020, Global Carbon Budget 2020, *Earth Syst. Sci. Data*, 12, 3269–3340, 2020, https://doi.org/10.5194/essd-12-3269-2020
38. Zhang, X. X., Sharratt, B., Lei, J. Q., Wu, C. L., Zhang, J., Zhao, C., Wang, Z. F., Wu, S. X., Li, S. Y., Liu, L. Y., Huang, S. Y., Guo, Y. H., Mao, R., Li, J., Tang, X. and Hao, J. Q., 2019, Parameterization schemes on dust deposition in northwest China: Model validation and implications for the global dust cycle, *Atmos. Environ.*, 209(April), 1–13, doi:10.1016/j.atmosenv.2019.04.017

39. Chappell, A., Webb, N., 2016, Using albedo to reform wind erosion modelling, mapping and monitoring, *Aeolian Research*, 23:63-78, http://dx.doi.org/10.1016/j.aeolia.2016.09.006